

The intestinal clock drives the microbiome to maintain gastrointestinal homeostasis

Received: 3 November 2021

Accepted: 23 September 2022

Published online: 14 October 2022

 Check for updates

Marjolein Heddes ^{1,2,5}, Baraa Altaha ^{1,2,5}, Yunhui Niu ^{1,2}, Sandra Reitmeier^{1,2}, Karin Kleigrewe ³, Dirk Haller ^{1,2} & Silke Kiessling ^{1,2,4} 

Diurnal (*i.e.*, 24-hour) oscillations of the gut microbiome have been described in various species including mice and humans. However, the driving force behind these rhythms remains less clear. In this study, we differentiate between endogenous and exogenous time cues driving microbial rhythms. Our results demonstrate that fecal microbial oscillations are maintained in mice kept in the absence of light, supporting a role of the host's circadian system rather than representing a diurnal response to environmental changes. Intestinal epithelial cell-specific ablation of the core clock gene *Bmal1* disrupts rhythmicity of microbiota. Targeted metabolomics functionally link intestinal clock-controlled bacteria to microbial-derived products, in particular branched-chain fatty acids and secondary bile acids. Microbiota transfer from intestinal clock-deficient mice into germ-free mice altered intestinal gene expression, enhanced lymphoid organ weights and suppressed immune cell recruitment. These results highlight the importance of functional intestinal clocks for microbiota composition and function, which is required to balance the host's gastrointestinal homeostasis.

Various physiological processes show 24-hour fluctuations. These rhythms are the expression of endogenous circadian (Lat. *circa* = about; *dies* = day) clocks that have evolved in most species¹ to facilitate anticipation of daily recurring environmental changes. In mammals, the circadian system includes a central pacemaker regulating sleep-wake behavior and orchestrating subordinated tissue clocks by humoral and neuronal pathways². At the cellular level, these clocks consist of inter-regulated core clock genes³ that drive tissue-specific transcriptional programs of clock-controlled genes (CCGs)⁴. Through these CCGs, circadian clocks regulate various aspects of physiology including metabolism, gastrointestinal transit time (GITT), mucus secretion, antimicrobial peptide secretion, immune defense and intestinal barrier function (reviewed by^{5–8}).

In mice, 10–15% of gut bacteria undergo diurnal oscillations in their abundance, influenced by meal timing, diet type and other environmental conditions^{9–11}. Recently, we found similar rhythms in

microbiota composition and function in population-based cohorts¹². Although functionality of the host's circadian system impacts microbial rhythmicity^{10,13,14}, it is unclear which tissue clocks contribute to this effect.

A balanced gut microbiome promotes health and microbial dysbiosis has been linked to metabolic diseases, colorectal cancer and gastrointestinal inflammation^{12,15–17}. Similar pathological consequences are associated with circadian rhythm disruption (reviewed by^{18–20}), which also induces microbiota dysbiosis^{10,11,13,14,21}. Consequently, we hypothesized that circadian regulation of microbiota composition and function may contribute to the host's gastrointestinal (GI) health.

Here, we functionally dissect the circadian origin of microbiota oscillations in mice. We provide evidence that intestinal epithelial cell (IEC) clocks generate the majority of gut microbial rhythms and their metabolic products, particularly short-chain fatty acids (SCFAs) and bile acids (BAs). Transfer of microbiota from IEC clock-deficient mice

¹ZIEL - Institute for Food & Health, Technical University of Munich, 85354 Freising, Germany. ²Chair of Nutrition and Immunology, Technical University of Munich, Gregor-Mendel-Str. 2, 85354 Freising, Germany. ³Bavarian Center for Biomolecular Mass Spectrometry, Technical University of Munich, Gregor-Mendel-Str. 4, 85354 Freising, Germany. ⁴Faculty of Health and Biomedical Science, University of Surrey, Stag Hill Campus, GU27XH Guildford, UK.

⁵These authors contributed equally: Marjolein Heddes, Baraa Altaha. ✉ e-mail: silke.kiessling@tum.de

in germ-free (GF) wild type hosts directly indicate the consequences of microbiota arrhythmicity and composition on the gastrointestinal homeostasis. Thus, we identify a mechanistic link between IEC clocks, gut bacteria rhythms and their functions through transfer experiments, showing the importance of gut clock controlled microbiota for host physiology.

Results

Rhythms in microbiota are generated endogenously by the circadian system

Diurnal rhythms in microbiota composition and function have been demonstrated in animal models and in humans^{9–12}. However, it has not been demonstrated whether these rhythms are a response to rhythmic external cues (*Zeitgebers*), such as the light-dark cycle, or are generated by endogenous clocks²² and, thus, persist when the organism is placed in an environment devoid of timing cues. To address this question, we compared fecal microbiota rhythms of the same wild-type mice kept in a rhythmic 12-hour light/12-hour dark (LD) cycle and constant darkness (DD) for two weeks (Fig. 1A). Host-driven rhythmic factors, which might influence microbiota composition, such as locomotor activity, food intake as well as total GITT, did not differ between light conditions (Supplementary Fig. 1A–D). 16 S rRNA profiling of fecal samples revealed clustering based on sampling time points rather than light condition (Fig. 1B, E). Generalized UniFrac distances (GUniFrac) quantification to ZTI identified rhythmicity in both light conditions (Fig. 1C). Importantly, 24-hour rhythms of species richness and Shannon effective number of species found in LD persisted in DD, supporting their circadian origin (Fig. 1D). Rhythms were also preserved in DD on phylum level with the two most dominant phyla Bacteroidetes and Firmicutes, oscillating in antiphase (Fig. 1E, F). Although microbiota composition is commonly analyzed by relative abundance, rhythmicity of highly abundant taxa may mask oscillations of small microbial communities, as previously demonstrated in fecal samples collected in LD¹³. Therefore, using synthetic DNA spikes, we performed relative quantification of the copy number of 16 S rRNA genes according to Tourlousee et al.²³, from here on referred to as ‘quantitative analysis’. With both approaches, highly abundant phyla and families, including *Lachnospiraceae* and *Muribaculaceae*, showed comparable circadian rhythmicity in LD and DD (Fig. 1F; Supplementary Fig. 1E). Few families, such as *Prevotellaceae* showed significant diurnal (LD), but no circadian (DD) rhythmicity, suggesting that their rhythms are regulated by the environmental LD cycle (Supplementary Fig. 1E). After removal of low-abundant taxa (mean relative abundance > 0.1%; prevalence > 10%), the remaining 580 zero-radius OTUs (zOTUs) displayed robust and comparable 24-hour oscillations in both light conditions, independent of the analysis (Fig. 1G, H; Supplementary Fig. 1F–I). The wide distribution of peak abundances, e.g., bacteria peaking during the day (mainly belonging to *Muribaculaceae*) and during the night (*Lachnospiraceae*) (Fig. 1G, H; Supplementary Fig. 1F–H), suggests that different microbial taxa dominate different daytimes. Importantly, more than 60% of all identified zOTUs were found to significantly oscillate in LD and in DD (Fig. 1G, H, Supplementary Fig. 1F–H, Supplementary data 1–3), suggesting that their rhythmicity is generated by the circadian system. Notably, comparable amounts of rhythmic zOTUs belong to the major phyla Firmicutes and Bacteroidetes (Supplementary data 2). Previous literature identified lower percentages of microbial rhythmicity^{9,10}. To assess this discrepancy we compared our results with the previously published data set from Thaiss and colleagues²⁴. Although the different methods to assign taxonomic units, namely OTUs (97% similarity strain assignment) in contrast to zOTUS (100% similarity strain assignment) caused disparity between amounts of rhythmic OTUs/zOTUs, the total abundance of rhythmic microbiota was comparable between both studies (Heddes et al.: 74%, Thaiss et al.: 83%, Supplementary Fig. 1L.

Supplementary data 4). Rhythmicity of the majority of zOTUs (e.g. the genera *Alistipes*, *Oscillibacter* and *Fusimonas*) identified in our study by relative analysis was further validated by quantitative analysis (73% in LD, 58% in DD) (Supplementary Fig. 1I, J). The diurnal rhythmicity found in 3/4 of all zOTUs examined in LD using JTK_CYCLE²⁵ is generated by the endogenous circadian system, since DODR analysis^{26,27} confirmed that more than 95% of zOTUs show similar rhythmicity in DD (e.g. the genera *Eubacterium* and members of the family *Lachnospiraceae*) (Fig. 1G; Supplementary Fig. 1K, Supplementary data 1, Supplementary data 3).

Robust microbial rhythms despite the absence of rhythmic food intake behavior

Light and food are the main *Zeitgeber* for the central and peripheral clocks, respectively^{2,28}. In our study, external light conditions only mildly effected microbial rhythms (Fig. 1) and previous research showed that rhythmic feeding time influences the phasing of microbiota rhythmicity^{10,11}. This prompted us to determine the dependency of bacterial oscillation on rhythmic food intake behavior by investigating microbiota rhythmicity in the absence of both *Zeitgeber* food and light. Therefore, we collected feces from starved mice during the 2nd day in DD (Fig. 2A). Although starvation altered microbial composition, clustering according to collection time points was significant in both feeding conditions (Fig. 2B, D). Microbiota diversity became arrhythmic in the absence of food (Fig. 2C). However, rhythms persisted in the two dominant phyla, highly abundant families, including *Muribaculaceae* and *Lachnospiraceae* and the majority of zOTUs (Fig. 2E–H, Supplementary data 1). Of note, circadian food intake behavior enhanced the amount of rhythmic zOTUs by 16% according to DODR analysis on quantitative data (Supplementary data 3). Nevertheless, circadian rhythms of highly abundant microbial taxa belonging to the families *Muribaculaceae* and *Ruminococaceae* maintained under starving conditions in both relative and quantitative analysis (Fig. 2E–I).

Together, these data show that although rhythms in gut bacteria are slightly influenced by environmental light and food conditions, intrinsic factors are the dominant drivers of circadian microbiota fluctuations.

The intestinal circadian clock controls microbiota composition and function

An important role of the host clock on diurnal microbiota fluctuation has previously been suggested based on experiments on mice with clock dysfunction in all tissues under LD conditions^{10,13,14}. The GI tract represents an important interface for cross-talk between IECs, bacteria and their metabolites²⁹ and thus might likely be involved in controlling microbiota composition. To identify the circadian origin of microbial rhythmicity, we used mice with IEC-specific deletion of the essential core clock gene *Bmal1* (*Bmal1^{IEC-/-}*). The rhythmic activity, food intake behavior as well as GITT and stool weight of *Bmal1^{IEC-/-}* mice did not differ from control littermates, reflecting a functional central pacemaker (Supplementary Fig. 2A–E). Arrhythmic core clock gene expression in the jejunum, cecum and proximal colon, in contrast to rhythms in the liver, confirmed intestine-specific clock ablation in *Bmal1^{IEC-/-}* mice (Supplementary Fig. 2F). Rhythmic genes relevant for host-microbe crosstalk, in particular *Tlr2*, *Muc2*, *Nfil3* and *Hdac3*^{30–35} lost rhythmicity in *Bmal1^{IEC-/-}* mice (Supplementary Fig. 2G). In line with this, microbiota composition in DD and LD differed significantly between *Bmal1^{IEC-/-}* mice and controls ($p = 0.037$ DD, $p = 0.018$ LD) and circadian rhythmicity in community diversity (species richness) observed in control mice was abolished in *Bmal1^{IEC-/-}* mice (Fig. 3A, B, Fig. 4A). Quantitative analysis revealed loss of rhythmicity of Firmicutes in *Bmal1^{IEC-/-}* mice in LD and DD (LD $p = 0.514$, DD $p = 0.313$), although, oscillation in relative abundance of the major phyla was found in both genotypes (Figs. 3C, Fig. 4C). Alterations in quantitative

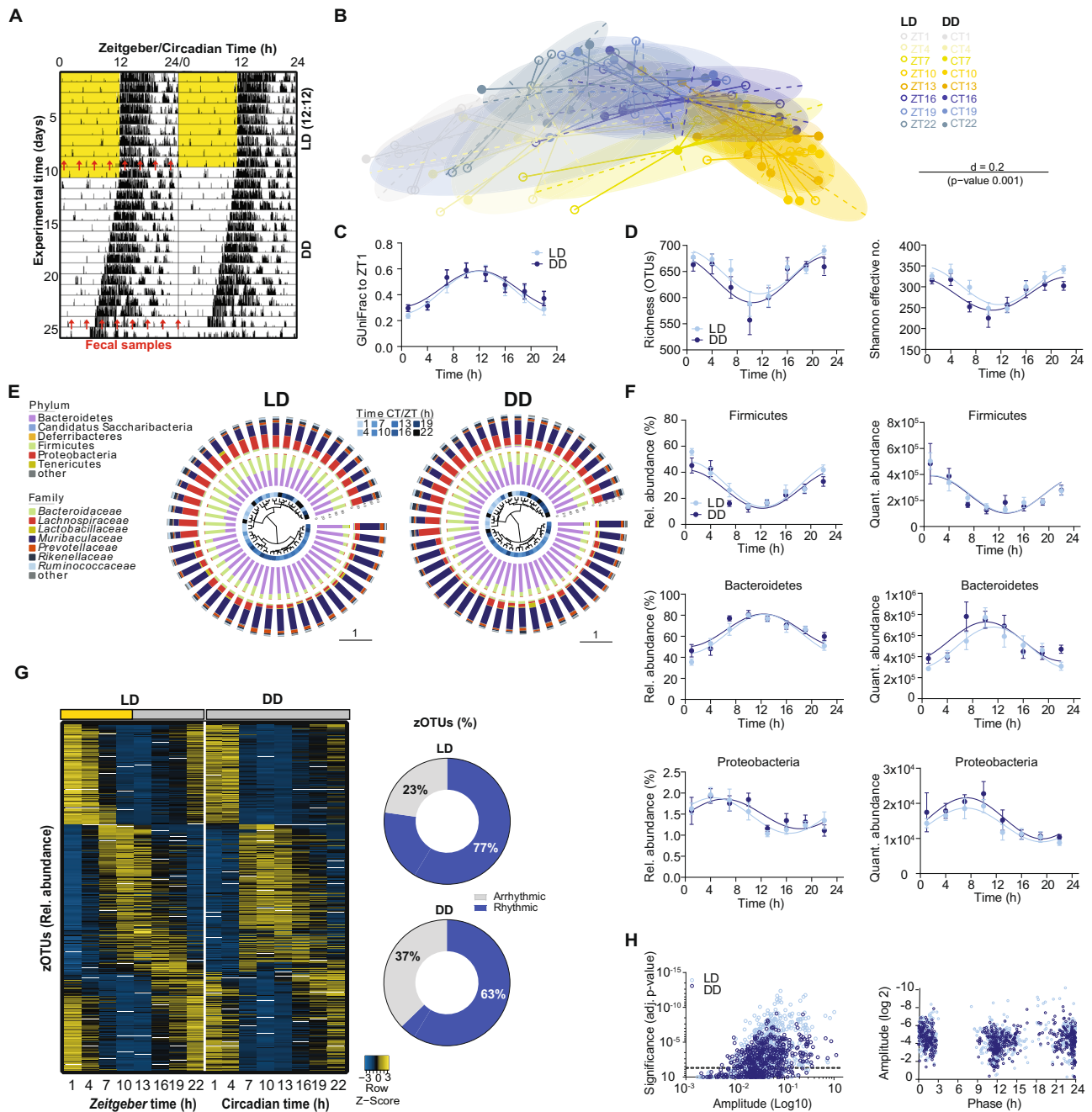


Fig. 1 | Fecal microbial rhythms persist in constant darkness. **A** Representative actogram of control (*Bmal1^{IEC1/ft}*) mice exposed to light-dark (LD) cycle and two weeks of constant darkness (DD). Fecal sampling times are indicated by red arrows. **B** Beta-diversity illustrated by MDS plots of fecal microbiota based on generalized UniFrac distances (GUniFrac) in LD and DD conditions. Significance was calculated with PERMANOVA with Bonferroni adjustment. **C** GUniFrac quantification over time relative to ZT1. **D** Diurnal (LD) and circadian (DD) profiles of alpha-diversity. **E** Dendrogram of microbiota profiles based on GUniFrac in LD and DD condition taxonomic composition at phylum and family level for each sample is shown as stacked bar plots around the dendrogram. The blue inner circle indicates the sampling time. **F** Diurnal (LD) and circadian (DD) profiles of the relative (left) and quantitative abundance (right) of phyla. **G** Heatmap depicting the relative

abundance of 580 zOTUs (mean relative abundance >0.1%; prevalence > 10%). Data are normalized to the peak of each zOTU and ordered by the peak phase in LD conditions. Z-score represents relative abundance where yellow means high abundance and blue low abundance. Pie-charts at the right indicate the amount of rhythmic (blue) and arrhythmic (grey) zOTUs identified by JTK_Cycle (Bonferroni adj. *p* value ≤ 0.05). **H** Significance (Bonferroni adj. *p*-value JTK) and amplitude of rhythmic and arrhythmic zOTUs (left) and phase distribution (right) in LD and DD based on relative analysis. Significant rhythms are illustrated with fitted cosine-wave regression using a solid line (significance: *p* value ≤ 0.05. LD (light-blue) and DD (dark-blue). *n* = 6 mice/time point/light condition. Data are represented as mean ± SEM. Source data are provided as a source datafile.

compared to relative rhythmicity analyses are not due to differences in 16 s copy number over time, as both genotypes show similar patterns in LD and DD conditions (Supplementary Fig. 2H, Fig. 4B). In accordance to results obtained from whole-body clock-deficient mice¹³, *IEC*-specific loss of *Bmal1* decreased the quantitative abundance of both

phyla, which was not visible in relative data sets (Fig. 3C, Fig. 4C). Similarly, rhythmicity observed in the relative abundance of families, including *Lachnospiraceae* and *Ruminococcaceae*, was abolished performing quantitative analysis (Supplementary Fig. 2I). Furthermore, dramatically disrupted circadian oscillations of *Bmal1^{IEC-/-}* mice in both

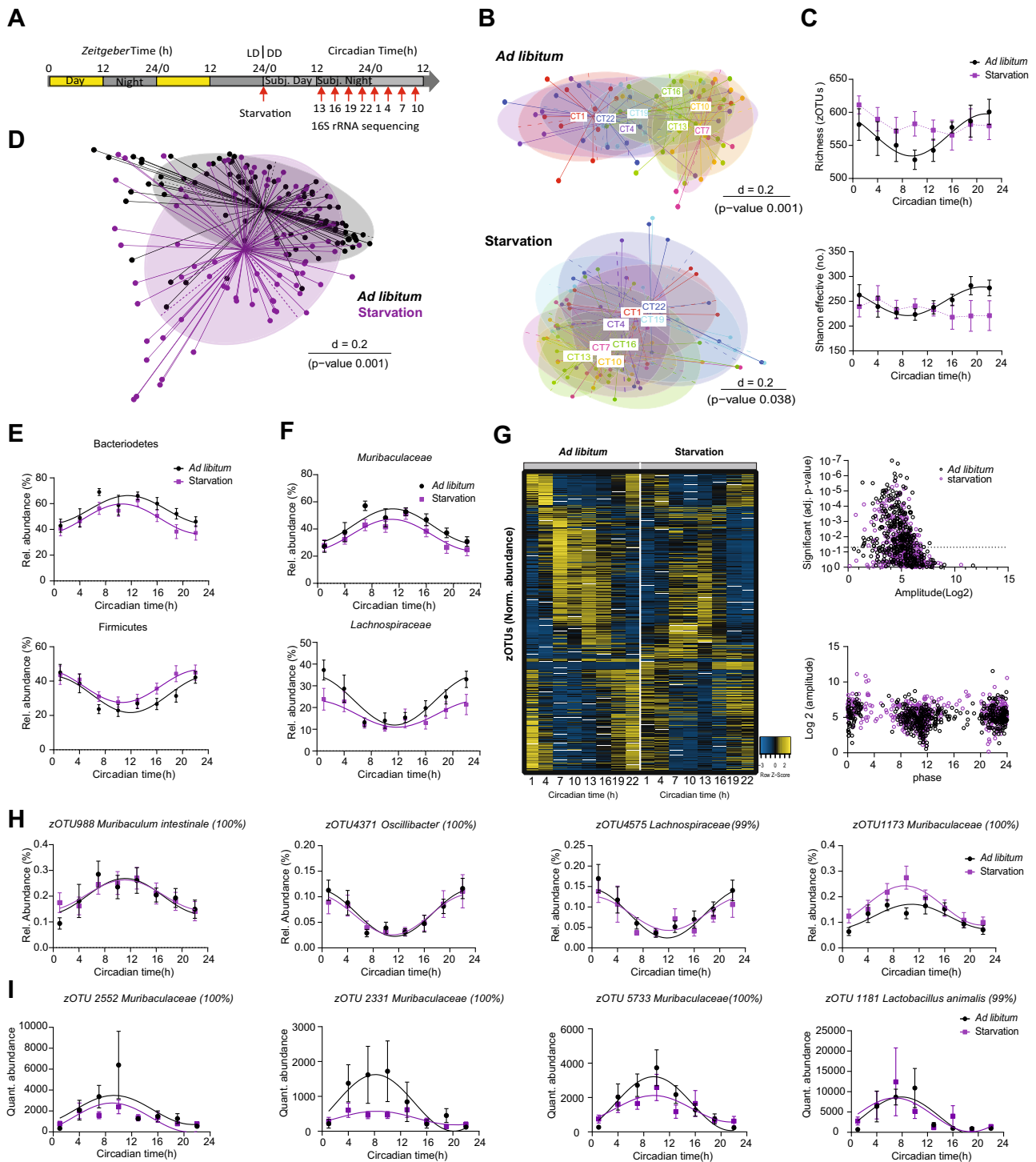
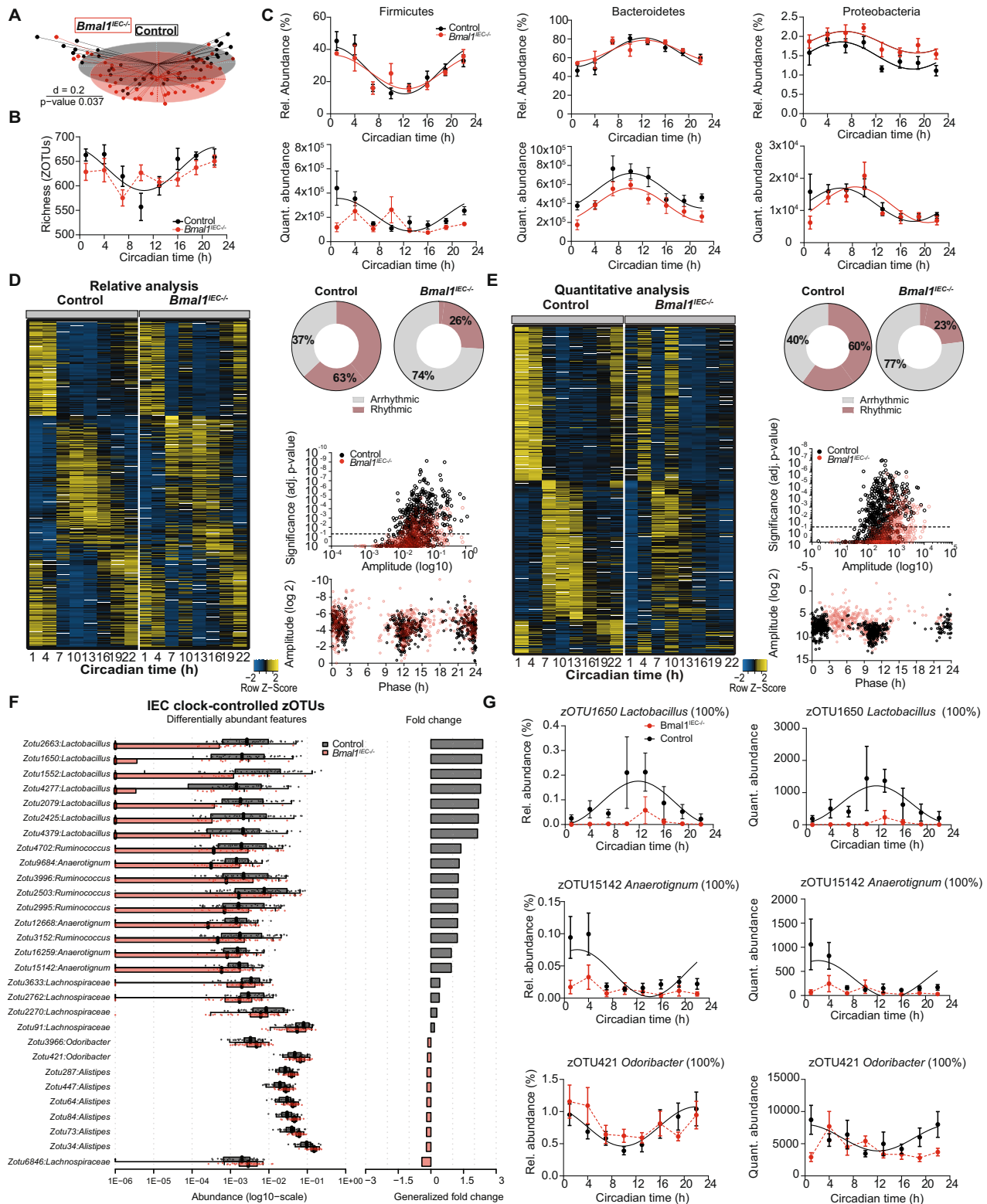


Fig. 2 | Food intake behavior marginally masks microbiota rhythmicity. **A** Schematic illustration of the experiment design. **B** Beta-diversity illustrated by MDS plot based on generalized UniFrac distances (GUniFrac) distances of fecal microbiota stratified by individual time points in *ad libitum* (top, black) and starvation (bottom, purple). **C** Circadian profiles of alpha-diversity. **D** PCoA plots of fecal microbiota based on GUniFrac distances stratified by feeding condition. **E, F** Circadian profiles of the relative abundance of the major phyla (**E**) and family (**F**) of fecal microbiota. **G** Heatmap depicting the relative abundance of 511 zOTUs (mean relative abundance > 0.1%; prevalence > 10%). Data are normalized to the peak of each zOTU and ordered by the peak phase in *ad libitum* condition. Z-score represents relative abundance where yellow means high abundance and blue low abundance. Significance and amplitude (JTK_Cycle analysis) of rhythmic and arrhythmic zOTUs (top) identified by JTK (Bonferroni adj. p value ≤ 0.05) and phase

distribution (based on cosine regression analysis) (bottom). Dashed line indicates adj. p value=0.05. **H, I** Circadian profile of relative (**H**) and quantitative (**I**) abundance of zOTUs of fecal microbiota. PERMANOVA test with Bonferroni adjustment to determine if the separation between group in **B & D** is statistically significant. Significant rhythms (cosine-wave regression, p value ≤ 0.05) are illustrated with fitted cosine-wave curves; data points connected by dotted lines indicate no significant cosine fit curves (p value > 0.05) and thus no rhythmicity. zOTUs were further analyzed with the adjusted compare rhythm script based on DODR. $n = 83$ *ad libitum* samples from 11 independent animals, 81 starvation samples from 11 independent animals for relative data in B-H (repeated measures). $n = 39$ *ad libitum* samples from 5 independent animals, 37 starvation samples from 5 independent animals for quantitative data in I (repeated measures). Data are represented by mean \pm SEM. Source data are provided as a source datafile.



relative and quantitative analyses was observed on the level of all 580 identified zOTUs illustrated by heatmaps (Fig. 3D, E). Of note, in *Bmal1^{IEC-/-}* mice the phase of remaining microbial oscillations was delayed using quantitative analysis (Fig. 3D, E). Based on both analyses more than 60% of fecal zOTUs, which account for more than two-third of bacterial abundance, underwent circadian oscillation in controls (Fig. 3D, E, Supplementary data 1). Importantly, the amount of rhythmic zOTUs was dramatically reduced by 2/3 in mice with IEC-specific *Bmal1* deficiency in both analyses, independent of the light conditions

(Fig. 3D, E, Fig. 4D, I, Supplementary data 1–3). Circadian zOTUs in control mice, which were arrhythmic in *Bmal1^{IEC-/-}* mice in both relative and quantitative analysis, belong predominantly to the families *Lachnospiraceae* and *Ruminococcaceae* of the phylum Firmicutes (Supplementary Fig. 3J, Supplementary data 2). The genera *Lactobacillus*, *Ruminococcus*, *Anaerotignum*, *Odoribacter* and *Alistipes* are among the taxa with differential rhythmicity comparing *Bmal1^{IEC-/-}* mice with their controls based on DODR analysis and in addition significantly differed in their abundance between genotypes (Fig. 3F, G).

Fig. 3 | The intestinal circadian clock drives circadian microbiota composition. **A** Beta-diversity illustrated by MDS plot of fecal microbiota based on generalized UniFrac distances (GUniFrac) stratified by genotype. Significance was calculated by PERMANOVA with Bonferroni correction. **B** Circadian profile of alpha diversity. **C** Circadian profile of relative (top) and quantitative (bottom) abundance of the major phyla. **D, E** Heatmap depicting the relative abundance (**D**) and quantitative abundance (**E**) of 580 zOTUs (mean relative abundance > 0.1%; prevalence > 10%). Data are normalized to the peak of each zOTU and ordered by the peak phase of control mice. Z-score represents relative abundance where yellow means high abundance and blue low abundance. Pie-charts at the right indicate the amount of rhythmic (colored) and arrhythmic (grey) zOTUs identified by JTK_Cycle (rhythmic = Bonferroni adj. p -value ≤ 0.05) based on relative (**D**) and quantitative (**E**) analysis. Significance and amplitude of rhythmic and arrhythmic zOTUs (top) and phase distribution (bottom) in controls and intestinal epithelial specific *Bmal1*-

deficient (*Bmal1*^{IEC-/-}) mice is depicted on the right of the heatmaps. Dashed line indicates p -value = 0.05. Bar charts in (**F**) represent the intestinal controlled zOTUs (Adj. compare rhythm script based on DODR abundance comparison between control and *Bmal1*^{IEC-/-} (two-sided Wilcoxon, adj. p -value < 0.05). Box and bar plots illustrate the alteration in quant. abundance (adj. p -value ≤ 0.05) and fold change of gut controlled zOTUs in the fecal samples with examples depicted in (**G**) Significant rhythms are illustrated with fitted cosine-regression solid lines; data points connected by dotted lines indicate no significant cosine fit curves (JTK Bonferroni adj. p -value > 0.05) and thus no rhythmicity. *Bmal1*^{IEC^{R/B}} controls (black) and *Bmal1*^{IEC-/-} (red). $n = 6$ (control);5(*Bmal1*^{IEC-/-}) mice/time point (**B,C,G**). $n = 48$ (control, 6 biological independent mice, repeated measures); 40(*Bmal1*^{IEC-/-}, 5 biological independent mice, repeated measures) (**A,D,E,F**). Data are represented as mean \pm SEM. Source data are provided as a source datafile.

Although the majority of zOTUs was under intestinal clock control, rhythmicity of around 20% of zOTUs (e.g. *Lactobacillus animalis* and *Pseudoflavonifractor*) persisted in *Bmal1*^{IEC-/-} mice (Fig. 3D, E, Supplementary data 1). To address whether these remaining rhythms were driven by the rhythmic food intake behavior observed in *Bmal1*^{IEC-/-} mice kept under ad libitum conditions in DD (Supplementary Fig. 2D), microbiota rhythmicity in *Bmal1*^{IEC-/-} mice was analyzed in feces from starved mice during the 2nd day in DD (Fig. 2A). Although beta diversity was significantly altered in the absence of rhythmic food intake, profiles of major phyla were undistinguishable between feeding conditions (Fig. 4E, F). Only a small amount of the remaining rhythmic zOTUs in *Bmal1*^{IEC-/-} mice significantly lost rhythmicity upon starvation based on DODR analysis (Supplementary data 3), such as bacteria belonging to *Turicimonas muris* and *Muribaculaceae* (Fig. 4G-I, Supplementary data 1).

Taken together, rhythmicity analyses of zOTU in *Bmal1*^{IEC-/-} mice and controls under different light and food conditions (Fig. 3, Fig. 4, Supplementary Fig. 2) highlight that the IEC clock represent the dominant driver of circadian gut microbiota oscillation.

Intestinal clock-controlled microbial functions balance gastrointestinal homeostasis

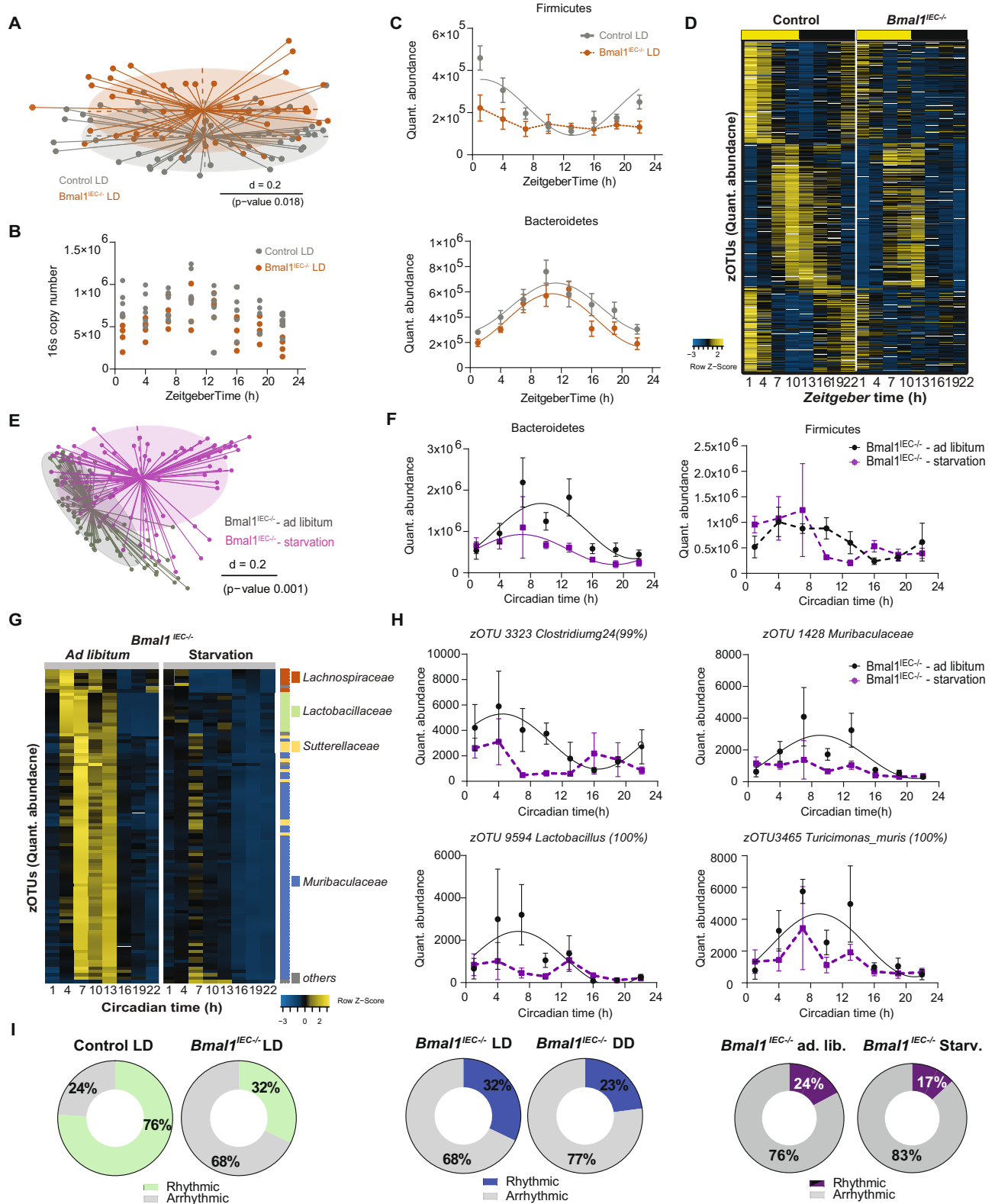
To address the potential physiological relevance of microbial oscillations, PICRUST 2.0 analysis was performed on intestinal-clock controlled zOTUs. Loss of microbial rhythmicity in *Bmal1*^{IEC-/-} mice was reflected in assigned pathways involved in sugar- and amino acid metabolism, vitamin biosynthesis and relevant for fatty acid (FA) metabolism such as β -oxidation, FA elongation and short-chain FA (SCFA) fermentation (Fig. 5A, Supplementary Fig. 3I). This prompted us to test the functional connection between intestinal clock-driven microbial rhythmicity and intestinal homeostasis (Fig. 5B–H). Indeed, Procrustes analyses (PA) identified an association between intestinal clock-controlled zOTUs and SCFA concentrations measured by targeted metabolomics ($p = 0.001$) (Fig. 5B). The level of valeric acid ($p = 0.04$, Mann-Whitney U test) and low-abundant branched-chain fatty acids (BCFAs) ($p = 0.01$, Mann-Whitney U test), including isovaleric, isobutyric, 2-methylbutyric differed between genotypes, although the amount of total and highly abundant SCFAs were comparable (Fig. 5C, Supplementary Fig. 3A). Nevertheless, concentrations of SCFAs negatively correlated with the relative abundance of intestinal clock-driven taxa, mainly belonging to the family *Muribaculaceae* of the phylum Bacteroidetes (Fig. 5D, Supplementary Fig. 3B). Positive significant correlations with multiple SCFAs, in particular BCFAs, were found with zOTUs belonging to the phylum Firmicutes, including the SCFA producers *Lachnospiraceae* and *Ruminococcaceae* (Supplementary Fig. 3B)³⁶. Similar to the results observed for SCFAs, associations were found between intestinal clock-controlled zOTUs and BAs levels ($p = 0.04$, Fig. 5G). Positive correlations with primary BAs and negative correlations with secondary BAs were observed with several intestinal clock-controlled taxonomic members mainly

belonging to Firmicutes (Fig. 5D, Supplementary Fig. 3D). For example, DHLCA and 7-sulfo-CA negatively correlated with *Oscillibacter* and *Eubacterium* (Fig. 5D, Supplementary Fig. 3D). In addition, almost half of the measured BAs differed among genotypes and, BAs, such as the conjugated primary BA, TCDA, and secondary BA, 7-sulfo-CA, lost rhythmicity in *Bmal1*^{IEC-/-} mice (Fig. 5E–F). Interestingly, most alterations were observed for secondary BAs (Fig. 5H, Supplementary Fig. 3C), which were linked to various GI diseases (reviewed by³⁷). In summary, these results indicate that deletion of intestinal clock function causes loss of rhythmicity in the majority of bacterial taxa and alters microbial functionality.

Transfer of arrhythmic intestinal clock-controlled microbiota disturbs GI homeostasis

To further test the physiological relevance of intestinal clock-driven rhythmic microbial composition and its functionality on host physiology, GF C57BL/6 mice were colonized with cecal content from *Bmal1*^{IEC-/-} or control mice ($n = 4$) (Fig. 6A). To confirm the importance of the gut clock in cecal microbial rhythmicity and composition, we performed 16 S sequencing as well as targeted metabolomics on cecal content of the donor mice. In line with results obtained from feces, 50% of the rhythmic zOTUs in the controls lost rhythmicity within cecal content of *Bmal1*^{IEC-/-} mice (Supplementary Fig. 4A–B). Moreover, several SCFA, including isovalerate and 2-methylbutyrate lost rhythmicity in *Bmal1*^{IEC-/-} mice cecal content (Supplementary Fig. 4C).

Importantly, ~76% of bacteria from the control and *Bmal1*^{IEC-/-} donor, were transferred into the recipients (Supplementary Fig. 3E). Reduced richness was observed in mice after microbiota transfer (Supplementary Fig. 3F), in line with previous reports³⁸. Interestingly, microbiota composition of recipient wild-type hosts significantly differed depending on the genotype of the donor (Fig. 6B; Supplementary Fig. 3G, H). Most of the transferred taxa belonged to Firmicutes, whose rhythmicity strongly depends on a functional intestinal clock, whereas abundances in Bacteroidetes were highly suppressed (Fig. 6C; Supplementary Fig. 3G). Importantly, lack of rhythmicity was transferred to mice receiving microbiota from *Bmal1*^{IEC-/-} mice (Fig. 6D, E). In particular rhythmicity of zOTUs belonging to e.g. *Alistipes*, shown to be driven by the gut clock (Fig. 3F) and maintained circadian rhythmicity in the host after transfer from control donors, lack rhythmicity in mice receiving microbiota from *Bmal1*^{IEC-/-} mice (Fig. 6E). Interestingly, after transfer of *Bmal1*^{IEC-/-}-associated arrhythmic microbiota several bacterial-derived metabolites, including BCFA as well as the secondary bile ketolithocholic acids were significantly upregulated and the primary BA β -muricholic acid (b-MCA) was significantly downregulated (Fig. 6F), similar to observations in made in donor mice (Fig. 5C, F, Supplementary Fig. 3A–D). Moreover, altered expression of intestinal clock genes in jejunum and colon was observed after transfer of arrhythmic microbiota in comparison to recipient mice receiving rhythmic microbiota (Supplementary Fig. 5A). In addition, the



expression of genes involved in host-microbe interaction, including *Arg2* and *Tlr4*, significantly differed depending on the genotype of the donor (Fig. 6G). *Bmal1^{IEC-/-}*-associated microbiota transfer induced the expression of *Il33* and *Nfkb* both known to be involved in intestinal inflammatory responses^{39,40} and reduced the expression of *Ang4* and *Hdac3* (Fig. 6G), which are known to integrate microbial and circadian cues relevant for inflammatory and metabolic intestinal functions^{31,33,35,41,42}. Although mesenteric lymph nodes and colon

weights of mice associated with arrhythmic microbiota were undistinguishable from controls and histology scores were unaffected, we noticed an increase in spleen and jejunum weight (Fig. 6H, Supplementary Fig. 5B, C), indicating a role of intestinal clock-controlled microbial on host intestinal homeostasis. Indeed, transfer of arrhythmic microbiota altered immune cell recruitment to the lamina propria. For example, an increase in dendritic cells (CD11c+) was detected in the small intestine whereas recruitment of T cells

Fig. 4 | Microbiota profiling of *Bmal1*^{IEC-/-} mice in light-dark conditions and under starvation. **A** Beta-diversity illustrated by MDS plot based on generalized UniFrac distances (GUniFrac) of fecal microbiota of *Bmal1*^{IEC-/-} (brown) and their *Bmal1*^{ECRfl} (grey) controls in LD conditions. Diurnal profiles of **(B)** 16 S copy number and **(C)** major phyla quantitative abundance. **D** Heatmap illustrating zOTUs quantitative abundance over time of fecal microbiota of *Bmal1*^{IEC-/-} and their controls in LD conditions. Data are ordered by the peak phase in LD conditions of the control group. **E** Beta-diversity principal coordinates analyses plot (PCoA) based on generalized UniFrac distances (GUniFrac) of fecal microbiota stratified by food availability. **F** Circadian profiles of phyla Firmicutes and Bacteroidetes. **G** Heatmap illustrating microbiota losing/changing rhythmicity after starvation in *Bmal1*^{IEC-/-} mice according to the adjusted compare rhythm script based on DODR (adj. *p* value ≤ 0.05). Data are normalized to the peak of each zOTU and ordered by the peak phase in *ad-libitum* condition. **H** Circadian profiles of the quantitative abundance of

example zOTUs masked by the food-intake behavior (adjusted compare rhythm script based on DODR, adj. *p* value ≤ 0.05). **I** Pie charts indicating the percentage of rhythmic/arrhythmic zOTUs in different condition according to JTK cycle analysis (rhythmic = JTK Bonferroni adj. *p* value ≤ 0.05). Significant rhythms (Cosine regression *p*-value ≤ 0.05) are illustrated with fitted cosine regression; data points connected by dotted lines indicate no significant cosine fit curves (*p*-value > 0.05) and thus no rhythmicity (**C, F, H**). zOTUs were further analyzed with the adjusted compare rhythm script based on DODR. Significance was calculated by PERMANOVA with Bonferroni adjustment (**A, E**). Ad libitum (black), starvation (purple). *n* = 6 (Control LD); 5 (*Bmal1*^{IEC-/-} LD)/time point (**B, C, D**). *n* = 43 independent Ad libitum samples from 6 independent animals, 44 independent Starvation samples from 6 independent animals (F-H). Data are represented as mean \pm SEM. Source data are provided as a source datafile.

(CD3 + CD4 +, CD3 + CD8 +) and dendritic cells (CD11c +) to the lamina propria of the colon was decreased (Fig. 6I, Supplementary Fig. 5D). Similar trends in immune cell recruitment and intestinal gene expression were observed in *Bmal1*^{IEC-/-} mice in SPF conditions (Supplementary Fig. 5E, F), suggesting that intestinal-clock controlled microbes influence gut immune homeostasis. Importantly, alterations found following transfer of *Bmal1*^{IEC-/-}-associated arrhythmic microbiota were not observed after transfer of microbiota from control mice kept in either LD, DD or starvation conditions, highlighting the physiological relevance of gut-clock-controlled microbiota (Supplementary Fig. 5G-I). Distinct gut microbial functionality controlled through food, light or the gut clock were further conformed through PICRUST analysis (Supplementary Fig. 6). In particular, a completely different metabolic signature was obtained in mice lacking a functional gut clock. For example, although loss of pathways in nucleotide metabolism was shared between conditions, loss of the gut clock additionally disrupts rhythmicity of pathways related to the TCA cycle and sugar metabolism (Supplementary Fig. 6). The profiles of LD and food regulated pathways were instead dominated by short chain fatty acid (SCFAs) metabolism, Amino acid metabolism and Vitamin, carrier and cofactor biosynthesis. In conclusion, our results support a different impact of the gut clock on microbial functionality compared to light and food.

Together, these results indicate that deletion of intestinal clock function caused loss of rhythmicity in the majority of bacterial taxa, alters microbial composition and functionality and resets the host's intestinal homeostasis.

Discussion

Diurnal microbial oscillations in the major phyla and families have previously been demonstrated in humans and mice by us and others⁹⁻¹³. Here we provide evidence that rhythmicity of the majority of these taxa persists even in the absence of external timing cues, demonstrating the endogenous origin of fecal bacterial circadian rhythms. In contrast, strongly attenuated microbial rhythms in cecal and ileal content were found in mice kept in DD⁴³. Differences in the amount and type of oscillating microbes between studies may be explained by variations in microbiota composition of the mouse lines, microbial ecosystem between facilities and niches within the GI tract. Moreover, our comparison analysis indicates that the discrepancy in total amounts of oscillating taxa between our study and previous studies^{9,10} is likely due to the different methods used to classify groups of closely related taxa. The comparability between studies may additionally be impacted by methodological differences, such as differences in the 16 S rRNA variable target gene region used for amplicon sequencing (here: V3-V4,⁴³; V4,¹⁰; V1-V2,²¹; V1-V3,⁴⁴; Metatranscriptome) as well as the sampling intervals (here: 3 h/day,⁴³; 6 h/day,¹⁰; 4 h/day).

Our results obtained from constant environmental conditions suggest that circadian microbiota regulation is primarily rooted in

host or bacterial intrinsic circadian mechanisms. Indeed, using IEC-specific *Bmal1*-deficient mice, we provide the first demonstration for a dominant role of intestinal clocks in driving fecal and cecal circadian microbiota composition. Lack of *Bmal1* in IECs led to dramatic loss of microbiota rhythmicity, predominantly belonging to the phylum Firmicutes, which was independent of whether relative or quantitative analyses was used. Of note, both microbiota analyses in this study did not always yield identical results, highlighting the importance of both analyses to interpret circadian microbiota composition. Microbiota composition is commonly analyzed by relative abundance; yet this analysis may exaggerate microbial rhythmicity due to masking by highly abundant taxa¹³. Arrhythmicity in taxa (e.g. *Lactobacillaceae*, *Odoribacteraceae* and *Lachnospiraceae*) was previously documented in mice lacking *Bmal1* or *Per1/2* tissues-wide^{10,13}. Loss of oscillations of the same taxa among others was observed in *Bmal1*^{IEC-/-} mice, identifying the IEC-clock to generate rhythmicity of these bacteria. This prominent role of the intestinal clock in driving microbial rhythmicity was further validate on data obtained in LD condition. Few of the remaining bacteria which were unaffected by IEC clock-deficiency, lost circadian rhythmicity upon starvation. Some of these taxa have previously been reported to be influenced by food availability¹¹. A prominent role for the timing of food intake on microbial rhythmicity was frequently suggested⁹⁻¹¹. However, we demonstrate that even in the absence of food, rhythmicity of dominant bacteria persisted, thus rhythmic food intake is not required to drive microbiota oscillations. Accordingly, in mice supplied with constant intravenous parenteral nutrition cecal microbiota composition oscillated⁹. Importantly, the majority of microbial rhythms was abolished in *Bmal1*^{IEC-/-} mice even though these mice show rhythmic food intake behavior. These results further highlight that IEC clocks are the dominant driver whereas environmental changes, as well as food-intake are mere modulators of microbial rhythms.

Mechanisms how intestinal clocks regulate microbiota rhythms likely involve local epithelial-microbe interactions and immune functions, including pattern recognition receptors, such as Toll-Like Receptors (TLRs), Aryl hydrocarbon receptors and nuclear receptors as well as antimicrobial peptide production and mucus secretion, all previously found to oscillate diurnally^{32,33,45}. Accordingly, we found IEC clocks to be essential for rhythmic expression of related genes, such as *Tlr2*, *Ang4*, *Muc2*, *Nfil3* and *Hdac3*, which are engaged in bidirectional microbe-host communication. For example, IEC-specific deletion of *Hdac3* or loss of *Tlr2* altered microbial composition and influenced intestinal homeostasis^{46,47}. Furthermore, *Muc2* can affect microbiota composition by allowing bacteria to metabolize mucin glycans⁴⁸, which through cross-feeding affects the abundance of other microbial taxa⁴⁹. However, future studies are required to functionally investigate intestinal clock mechanism controlling microbiota composition.

Circadian disruption due to life style has been correlated to microbiota dysbiosis and human health (reviewed by⁵⁰). Recently, we

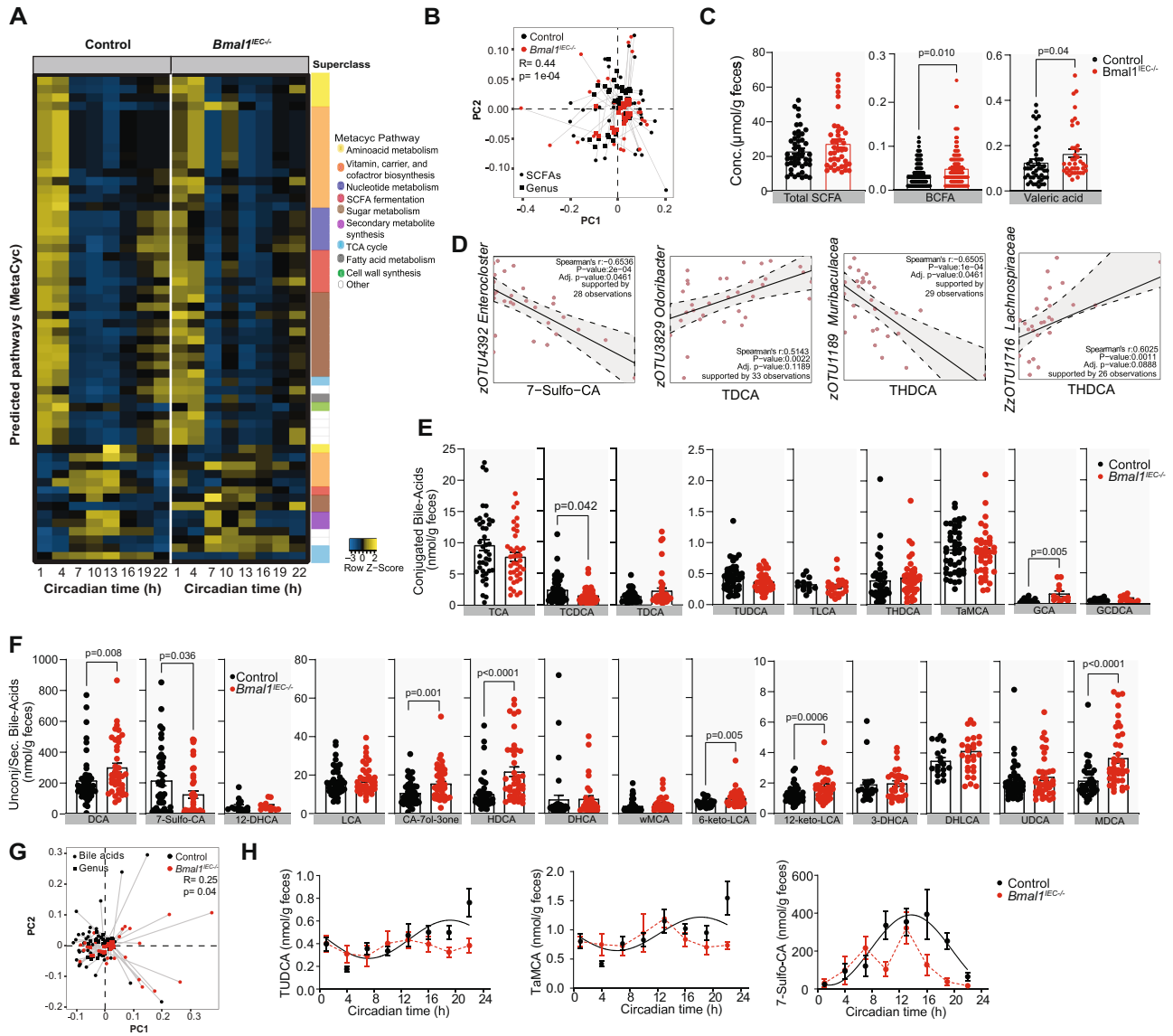


Fig. 5 | Metabolic functioning of intestinal clock-controlled bacteria.

A Heatmap of MetaCyc Pathways predicted using PICRUST2.0 on intestine clock-controlled zOTUs rhythmic in control (left) and arrhythmic in *Bmal1^{IEC/-}* (right) mice. Pathways are colored according to their subclass. **B** Procrustes analyses (PA) of fecal microbiota and SCFA levels. The length of the line is proportional to the divergence between the data from the same mouse. **C** SCFA concentrations in feces. **D** and Spearman correlation (p value ≤ 0.05 and $R \leq -0.5$; red or $R \geq 0.5$; blue) between SCFA and gut controlled bacteria taxa. **E** Conjugated and secondary (**F**) fecal BAs levels. **G** PA as described in (**D**) with fecal bile-acid (BA) levels. **H** Circadian profiles of BAs. Significant rhythms are illustrated with fitted cosine-regression (solid line); data points connected by dotted lines indicate no significant cosine fit curves (p value > 0.05) and thus no rhythmicity. $n = 5$ (*Bmal1^{IEC/-}*); 6 (control)/time point (**H**). $n = 40$ (*Bmal1^{IEC/-}*), 5 biological independent samples), 48 (Control), 6 biological independent samples), repeated measures (**C**, **E**, **F**). Control (black) and

Bmal1^{IEC/-} (red). Data are represented as mean \pm SEM. Significance was calculated with two-sided Mann-Whitney U test (**C,E,F**). BCFA = branched-chain fatty acids. Cholic acid (CA), α -Muricholic acid (aMCA), β -Muricholic acid (bMCA), Taurocholic acid (TCA), Taurochenodeoxycholic acid (TCDCA), Tauroursodeoxycholic acid (TUDCA), Taurohydrodeoxycholic acid (THDCA), Tauroolithocholic acid (TLCA), Taurodeoxycholic acid (TDCA), Tauro- α -Muricholic acid (TaMCA), Glycochenodeoxycholic acid (GidCDA), Glycocholic acid (GCA), Deoxycholic acid (DCA), Lithocholic acid (LCA), γ -Muricholic acid (γ -MCA), 12-Dehydrocholic acid (12-DHCA), 12-Ketolithocholic acid (12-keto-LCA), 3-Dehydrocholic acid (3-DHCA), 6-Ketolithocholic acid (6-keto-LCA), 7-Dehydrocholic acid (7-DHCA), 7-Sulfocholic acid (7-sulfo-CA), Allocholic acid (ACA), Cholic acid-7 α -3one (CA-7 α -3one), Ursolic acid (UCA), Dehydrolithocholic acid (DHLCA), Hyodeoxycholic acid (HDCA), Murideoxycholic acid (MDCA), Ursodeoxycholic acid (UDCA). Source data are provided as a source datafile.

found a functional link between arrhythmicity of microbiota and the development of obesity and T2D¹². Here we demonstrate intestinal-clock dependent rhythmicity of taxa involved in SCFA fermentation, such as *Lachnospiraceae*, *Ruminococcaceae* and *Odoribacteraceae*, lactate acid producing bacteria e.g. *Lactobacillaceae*, mucus foragers, such as *Muribaculaceae*, *Rickenellaceae* and *Lachnospiraceae*^{36,51,52}. Moreover, taxa capable to convert bile acids (BAs), including *Lactobacillus* and *Ruminococcus*⁵³ are regulated by intestinal circadian clocks. Consequently, IEC clocks likely influence microbiota function.

Indeed, functional analysis based on 16S rRNA gene data revealed pathways such as SCFA fermentation, amino-acid and carbohydrate metabolism are associated to intestinal clock-controlled taxa. Many among the identified pathways were shown to diurnally oscillate in healthy individuals, to lose rhythmicity in clock deficient mice, and are associated with host's health^{10,12,54}. Targeted metabolite analysis further confirmed that arrhythmicity in intestinal clock-controlled taxa is reflected in alterations of key metabolites involved in lipid signaling pathways such as SCFAs and BAs. Both of these microbiota-related

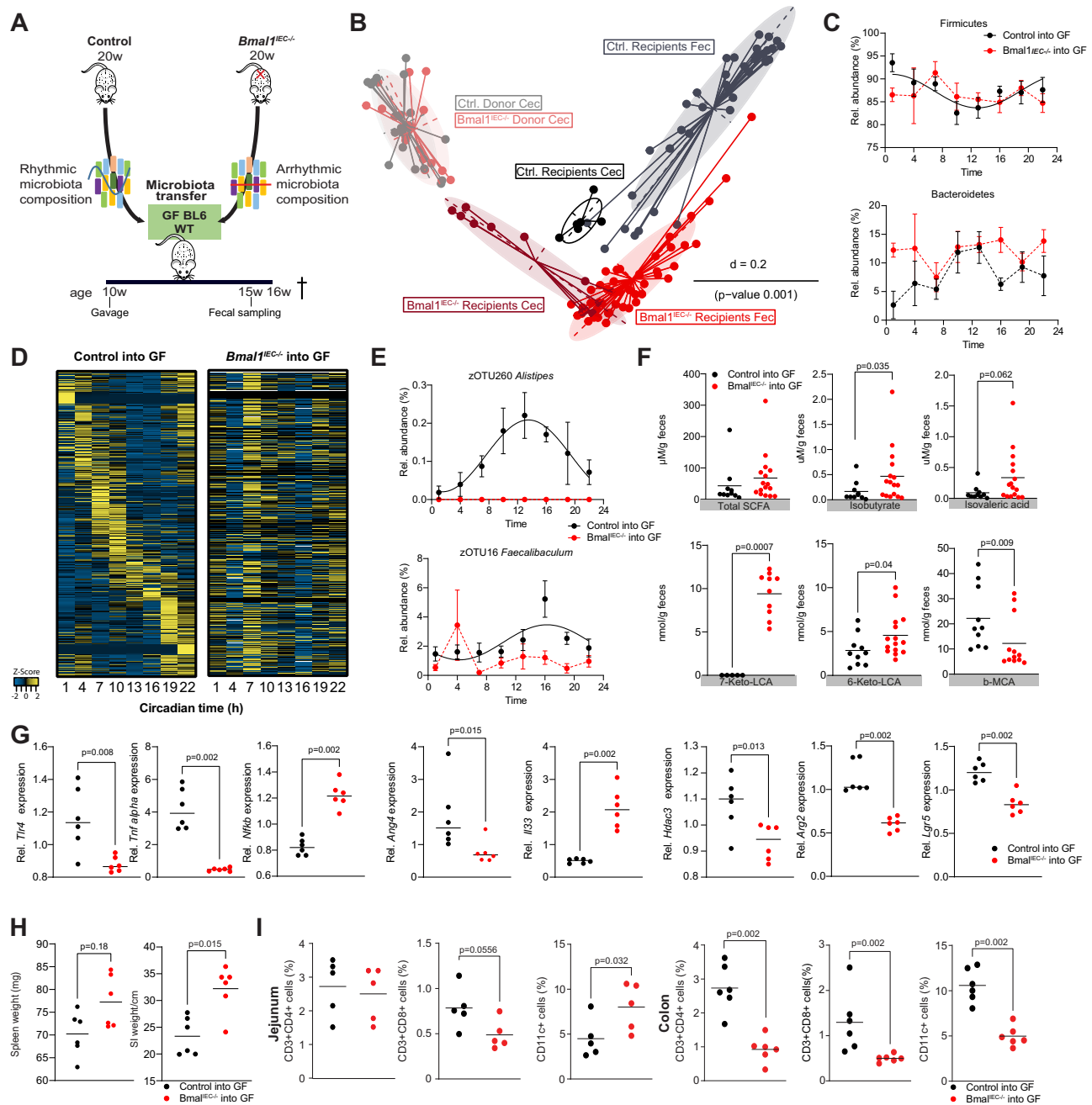


Fig. 6 | Intestinal clock-controlled microbiota are essential for intestinal homeostasis. **A** Schematic illustration of transfer experiments with mixture of cecal microbiota obtained from *Bmal1^{IECfl/IECfl}* control and *Bmal1^{IEC-/-}* donors ($n = 4$) into 10 weeks old germ-free BL6 wild-type recipient mice till sacrifice at 16 weeks (16w). Fecal profiles were collected 5 weeks after gavage at the age of 15 weeks (15w). **B** MDS plot of GUniFrac distances of donor (CT13) and recipient mice ($n = 6$ /genotype/time point) after 5 weeks of transfer. Significance was calculated by PERMANOVA with Bonferroni correction. **C** Diurnal profiles of fecal microbiota at phylum level. **D** Heatmap depicting the relative abundance of zOTUs ordered by their cosine-regression peak phase according to the recipient controls. On the left the first two columns indicate donor zOTU abundance. **E** Diurnal profile of relative

abundance of example zOTUs. **F** Fecal SCFA and BAs concentrations. **G** Relative gene expression of *Trf4*, *Arg2*, *Ang4*, *Trnfa*, *Il33*, *Nfkb*, *Hdac3*, *Lgr5* in the proximal colon of recipient mice of control (black) or *Bmal1^{IEC-/-}* (red) cecal microbiota. **H** Organ weights of recipient mice after receiving control (black) or *Bmal1^{IEC-/-}* (red) cecal microbiota. **I** Frequency of CD3 + CD4 +, CD3 + CD8 +, CD11c + cells in jejunum rhythms are illustrated with fitted cosine-regression; data points connected by dotted lines indicate no significant cosine fit curves (p value > 0.05) and thus no rhythmicity. $n = 6$ mice/genotype. Data are represented as mean \pm SEM. Significance was calculated by Mann-Whitney U test, two-sided (**F**, **G**, **H**, **I**). Source data are provided as a source datafile.

metabolites are known to diurnally oscillate and impact, among others host immune and metabolic functioning^{9,55–59}. Notably, high levels of secondary BAs, e.g. DCAs and HDCAs identified in *Bmal1^{IEC-/-}* mice, were also found in subjects with metabolic disorders including obesity and T2D^{60–63}. Moreover, TUDCA lost circadian rhythmicity in *Bmal1^{IEC-/-}* mice and was found to ameliorate insulin sensitivity in both obese mice

and humans^{64,65}. In addition, the accumulation of BAs within the host has been associated with several GI diseases. For example, increased levels of the sec. BA DCA and taurine-conjugated BAs were linked to colorectal cancer in mice (reviewed by Jia and colleagues⁶⁶). These results support the hypothesis that a functional intestinal clock balances GI health by driving microbial function.

Transfer experiments provide direct evidence for the physiological relevance of intestinal clock-controlled microbiota and their functions. Depending on the donor genotype microbiota transfer induced molecular and physiological changes in the healthy hosts. Notably, a functional intestinal clock in recipients seems to require longer than 5 weeks to restore microbial rhythmicity, suggesting strong microbe-host clock interactions. Indeed, this was supported by altered clock gene expression in recipients receiving arrhythmic microbiota and is in accordance with a report indicating a role of microbial rhythmicity in programming host transcriptome rhythmicity²⁴. Additionally, the alteration of microbial metabolite production in recipients, which reflect the results obtained from donor mice, e.g. upregulated BCFAs and sec. BAs, may have influenced intestinal clock functions, since a direct impact on rhythmicity in intestinal epithelial cells and subsequent metabolic responses in the host has been provided previously^{9,48}. Of note, gut-clock deficiency causes microbial arrhythmicity, but slight changes in microbiota composition were observed. Thus, we cannot rule out the possibilities that changes in recipients following microbiota transfer might be caused due to compositional changes rather than rhythmicity. However, recipients show rhythmicity and arrhythmicity depending on the donor genotype, indicating that the alterations observed in recipients following microbiota transfer are likely caused by changes in microbial rhythmicity.

Transfer of microbiota from intestinal clock-deficient mice altered several genes involved in inflammation, antimicrobial peptide production and intestinal epithelial functioning including *Trnf- α* , *Tlr2*, *Lgr5*, *Ffar2*, *Hdac3* and *Nf-kB*^{39–41,67–70}. Changes in the expression of these genes due to reception of *Bmal1*^{IEC-/-}-associated microbiota might have caused the observed immune phenotype in recipients. For example, *Tlr2* senses the presence of microbe-associated molecular patterns and is capable to regulate the host's immune system against pathogenic infiltration by regulating *Trnf- α* cytokine production of CD8 + T-cells^{71,72}. Moreover, *Hdac3* and *Il33* also plays an important role in microbe-host crosstalk^{46,73}. Mouse models lacking HDAC3 show high susceptibility to DSS-induced inflammation, partly by activation of NF- κ B, the latter also observed in our mouse model^{146,74}. Consequently, altered regulation of *Tlr2*, *Trnf- α* , *Hdac3*, and *Il-33* expression observed in mice receiving microbiota from *Bmal1*^{IEC-/-} mice, likely disturbed gastrointestinal homeostasis. Indeed, enhanced lymphoid tissues weight and suppressed recruitment of T-cell and dendritic cell populations to the lamina propria within the colon was found in GF mice receiving microbiota from intestinal clock-deficient mice. Immune cell recruitment represents an important aspect in the gastrointestinal immune defense (reviewed by⁷⁵). Interestingly, we observed similar alterations and microbial-derived metabolite changes in recipients and SPF donors, indicating that microbiota might transfer the phenotype from the donor to recipients. Discrepancies between the immune phenotype observed in donor and recipient mice might be caused by genetic loss of *Bmal1* in the intestine of donors and feedback from arrhythmic microbiota on intestinal tissue of rhythmic recipients. In contrast, transfer of microbiota from control mice kept in LD, DD or in starving conditions did not cause the same alterations in immune cell recruitment, gene expression or microbial metabolites levels. These results provide the first evidence that intestinal clock-controlled gut bacteria are crucial for a balanced intestinal immune homeostasis, and likely influence the immune response to pathogens, infection and inflammation.

Taken together, a functional intestinal clock represents a key element to maintain gastrointestinal health by driving rhythmicity of gut bacteria and microbial products. Since intestinal clock functions effect bacterial taxa required for a balanced immune defense, it remains to be studied whether arrhythmicity of intestinal clock-controlled taxa is causal for the development of gastrointestinal diseases. In the scope of previous associations of arrhythmic microbiota and their products with T2D and IBD^{12,76}, our data highlight the

relevance to further investigate intestinal clock mechanisms driving bacterial rhythmicity for human health.

Methods

Ethics statement

Experiments were conducted at Technical University of Munich in accordance with Bavarian Animal Care and Use Committee (TVA ROB-55.2Vet-2532.Vet_02-18-14).

Mouse models

***Bmal1*^{IEC tg/wt} and *Bmal1*^{IECfl/fl} mouse generation.** Male epithelial intestinal epithelial cell-specific *Bmal1* knock-out (*Bmal1*^{fl/fl} x Villin CRE/wt; referred to as *Bmal1*^{IEC-/-}) mice and their control littermates (*Bmal1*^{fl/fl} x Villin wt/wt; referred to as *Bmal1*^{fl/fl}) on a genetic C57BL/6J background were generated as previously described⁷⁷. Breeding was performed by crossing *Bmal1*^{fl/fl} x Villin CRE/wt with *Bmal1*^{fl/fl} x Villin wt/wt. Unless otherwise stated, mice were kept in LD 12:12 cycles (300 lux), with lights turned on at 5am (*Zeitgeber* time (ZT0)) to 5 pm (ZT12). All mice were single housed at the age of 8 weeks in running wheel-equipped cages with ad libitum access to chow diet (V1124-300, Ssniff Diets, Soest, Germany) and water under specific-pathogen free (SPF) conditions according the FELASA recommendation at 22 ± 1 °C. In order to minimize cage-related bias in microbiota composition⁷⁸, littermates and litters of comparable age from as few as possible breeding pairs and cages were selected.

Behavior analysis

All male mice, unless stated otherwise, were individually housed in cages with running wheels. Handling and activity measurements during experiments were performed as described⁷⁹. Wheel-running activity was analyzed using ClockLab software (v6.0.52, Actimetrics). The last 10–14 days of each condition were used to determine the period (tau, calculated using a X² periodogram and confirmed by fitting a line to the onsets of activity), the duration of the active period (alpha), the amount of activity and the subjective day/night activity ratio (where the subjective day under DD conditions is the inactive period between the offset of activity and the onset of activity and the subjective night is the active period between the onset of activity and the offset of activity).

Light-dark (LD) and constant darkness (DD) conditions and fecal sample collection

Male *Bmal1*^{IEC-/-} and their control littermates *Bmal1*^{IECfl/fl} ($n = 6$ /genotype) were maintained under LD cycle for 2 weeks (age 8–10 weeks), switched to a DD cycle for 2 more weeks (age 10–12 weeks), kept in constant light (LL) for an additional 2 weeks (age 12–14w) and finally returned back to LD till the age of 18–20 weeks before sacrifice. Average daily food intake was measured over 5 consecutive days in the second week of the above indicated light conditions. Of note, Fecal sample collection in darkness was performed after adjusting for each mouse's individual free-running period (Supplementary Fig. 2A). For example, the activity period varied by -0.5 hours per day within mice of the same genotype and consequently accumulates to a -7-hour phase difference between individual mice after 2 weeks in DD. Fecal collection in LD was performed according to normal *Zeitgeber* time. Samples were collected every 3 hours over the course of a 24h-day (Fig. 1A, Supplementary Fig. 2A).

Food deprivation

Eleven-week-old *Bmal1*^{IEC-/-} and control male mice ($n = 11$) with *ad libitum* food intake were used for fecal sample collection. At the age of 12–13 weeks, *Bmal1*^{IEC-/-} mice ($n = 12$) and their control ($n = 11$) littermates were starved beginning at CT1 on the 1st day in DD. Fecal samples were collected as detailed above starting at CT13 on the 2nd day in DD (after 13 hours of starvation) till CT10 (after 34 hours of starvation) at the indicated time points (Fig. 2A).

Food intake pattern and analysis

The diurnal food intake pattern of individually housed mice was recorded using an automated monitoring system (TSE LabMaster Home Cage Activity, Bad Homburg, Germany) at the age of 10–12 weeks. Mice were habituated for 3 days. Then data were collected for a full 24-hours profile at the 4th day. Cumulative food intake was recorded through high precision balances connected to the food baskets. Food basket weight were summed up in 1 min intervals. Total food intake was calculated as 1st derivative of cumulative food intake and consumption was summed up at intervals of 1 hour. One-minute intervals where the weight loss was directly followed by a similar weight gain in food baskets within a period of 3 minutes were excluded. Circadian food intake of individually housed mice was recorded in the second day of darkness by weighing the food every 3 h.

Complete gastrointestinal transit time

Complete GI transit time (GITT) was measured by administering natural carmine red (6%, Sigma Aldrich) dissolved in 0.5% methylcellulose (Sigma-Aldrich) by gavage (100ul) according to⁸⁰. 16–18 week-old male *Bmal1*^{IEC-/-} and *Bmal1*^{fl/fl} mice were starved 6 h prior to gavage. Time of gavage was considered T0. In case of presence, fecal pellets were taken out of the cage every 10 minutes and checked for red color. GITT was registered as the time between T0 and the time of presence of carmine red in the fecal pellets.

Tissue collection in SPF conditions

All animals were sacrificed by cervical dislocation at the age of 18–20 weeks in the second day of darkness at the indicated circadian times (CT) or in LD12:12 conditions, in 4 h intervals starting at 1 hour after lights off (ZT1). In constant darkness samples were collected at the indicated time points used for control mice in LD. Eyes were removed prior to tissue dissection. Tissues were harvested and snap frozen on dry ice and stored in –80 degrees.

Gene expression analysis (qRT-PCR) quantitative real-time PCR

RNA was extracted from snap frozen tissue samples with Trizol reagent. cDNA was synthesized from 1000 ng RNA using cDNA synthesis kit Multiscribe RT (ThermoFischer Scientific). qPCR was performed in a Light Cycler 480 system (Roche Diagnostics, Mannheim, Germany) using Universal Probe Library system according to manufacturer's instructions. For genes expression the following primers and probes were used: Brain and Muscle ARNT-Like 1 (*Bmal1*) F 5'-ATCCAGGGGAACCAGA-3' R 5'-GGCGATGACCCTTATCC-3' Probe 15, Period 2 (*Per2*) F 5'-TCCGAGTATATCGTGAAGAAGC-3' R 5'-CAGGATCTTCCAGAAACCA-3' probe 5, Nuclear receptor subfamily 1 group D member 1 (*Reverba*) F 5'-AGGAGCTGGGCTATTCAC-3' R 5'-CGGTTCTCAGCACCAGAG-3' probe 1, Toll-like receptor 2 (*Tlr2*) F 5'-GGGGCTTCACTTCTGTGCTT-3' R 5'-AGCA TCCTCTGAGATTTGACG-3' probe 50, Angiogenin 4 (*Ang4*) F 5'-CCCCAGTTGGAGGAAAGC-3' R 5'-CGTAGGAATTTTTCTGACCTTTCA-3' probe 106, Mucin 2 (*Muc2*) F 5'-GGCAGTACAAG AACCGGAGT-3' R 5'-GGTCTGGCAGTCCTCGAA-3' probe 66, Histone Deacetylase 3 (*Hdac3*) F 5'-GAGAGGTC CCGAGGAGAAC-3' R 5'-CGCCATCATAGAATCATTGG-3' probe 40, Tumor necrosis factor alpha (*Tnfa*) F 5'-TGCCTATGTCTCAGCCTTTC-3' R 5'-GAGGCCATTTGGGAATTCT-3' probe 49, Leucine Rich Repeat Containing G Protein-Coupled Receptor 5 (*Lgr5*) F 5'-CTTCACTCGGTGCACTGCT-3' R 5'-CAGCCAGCTACCAATAGGTG-3' probe 60, Toll like receptor 4 (*Tlr4*) F 5'-GGACTCTGATCATGGCACTG -3' R 5'-CTGATCCATGCATTGGTAGGT-3' probe 2, Nuclear factor kappa-light-chain-enhancer of activated B cells (*Nfkb*) F 5'-CCCAGACCGCAGTATCCAT -3' R 5'-GCTCCAGGTC TCGCTTCTT-3' probe 47. RNA abundance was normalized to the housekeeping gene Elongation factor 1-alpha (*Efla*) F 5'-GCCAATTTCTGGTTGGAATG-3' R 5'-GGTGACTTTCCATCCCTTGA-3' probe 67. For Interleukin33 (*Il33*) gene was used sybr green to run the gene using the following primer F 5'-GAACATGAGTCCCATCAAAG -3' R 5'-CAGC

TGGTTATCTTTACTCC -3' and RNA abundance was normalized to the housekeeping gene *Efla* F 5'-GCCAAT TTCTGGTTGGAATG-3' R 5'-GGTGACTTTCCATCCCTTGA-3'.

High-throughput 16 S ribosomal RNA (rRNA) gene amplicon sequencing analysis

Genomic DNA was isolated from snap-frozen fecal pellets according to a modified protocol of Godon and colleagues⁸¹, as previously described¹². DNA NucleoSpin gDNA columns (Machery-Nagel, No. 740230.250) were used for DNA purification. In a two-step PCR the V3-V4 region (using the primers 341F-ovh and 785r-ov) of the 16 S rRNA gene was amplified from 24 ng DNA. After pooling, the multiplexed samples were sequenced on an Illumina HiSeq in paired-end mode (2×250 bp) using the Rapid v2 chemistry, in accordance with¹². Two negative controls, consisting of DNA stabilizer without stool, were used for every 45 samples to control for artifacts and insure reproducibility. High-Quality sequences of read counts > 5000 were used for 16 s rRNA data analysis. Reads FASTQ files were consequently processed using an in-house developed NGSToolkit (Version Toolkit 3.5.2_64) based on USEARCH II⁸². A trim score of 5 was used on the 5' end and 3' end for the R1 and R2 read followed by chimera removal⁸³ using the FASTQ mergepair script of USEARCH⁸². Quality filtered reads were merged, deduplicated, clustered and a denoised clustering approach was applied to generate zero-radius operational taxonomic units (zOTUs)^{82,84}. Using zOTUs analysis provide the best possible resolution considering the 16 s rRNA sequencing, by correcting the sequencing error (denoising step) and then identifying each unique sequence (100% similarity) as a different microbial strain. On the other hand, previously OTU analysis was used, which is based on merging different strains which has more than 97% similarity into one single OTU, and assign it to one microbial strain⁸⁵. Taxonomic assignment was performed with the EZBioCloud database⁸⁶. Notably, For Supplementary Fig. 1L Taxa were assigned to Greengenes database in order to be able to compare our results with the data obtained in the study by Thaiss and colleagues¹⁰. Data was further analyzed with the R-based pipeline RHEA⁸⁷. Phylogenetic trees are generated by a maximum likelihood approach, which was performed on an alignment generated by MUSCLE with the software MegaX⁸⁸. Trees were visualized and annotated with the use of the online tool EvolView (<http://www.evolgenius.info/evolview/>)⁸⁹. Spike-in of 12 artificial DNA standards mimicking 16 S rRNA genes (a surrogate for bacterial numbers) were used to determine the quantitative copy numbers of rRNA genes per gram of fecal sample between samples. Briefly, the same amount of artificial DNA (6 ng) was added to each weighted fecal sample before DNA extraction. After sequencing as described above, FASTQ files were mapped against the spike FASTA sequences (using bowtie2), removing the spike reads and generating a new FASTQ file. By comparing the spike sequencing reads to the fecal bacterial reads; we calculate the quantitative number of 16 S rRNA gene copies per gram of sample. The copy number of 16 S rRNA gene is proportional to the number of bacteria present in a sample. Thus, this approach enables estimation of microbial abundances relative between samples, suitable for comparative analysis according to Tourlousse et al. 2017²³.

Targeted metabolite analyses

Sample preparation for targeted metabolite analyses. Approximately 20 mg of mouse fecal pellet was weighed in a 2 mL bead beater tube (CKMix 2 mL, Bertin Technologies, Montigny-le Bretonneux, France) filled with 2.8 mm ceramic beads. 1 mL of methanol-based dehydrocholic acid extraction solvent (c = 1.3 μmol/L) was added as an internal standard for work-up losses. Fecal samples were extracted with a bead beater (Precellys Evolution, Bertin Technologies) supplied with a Cryolys cooling module 3 times each for 20 seconds with 15 seconds breaks in between at 10.000 rpm.

Targeted bile acid measurement. 20 μL of isotopically labelled bile acids (ca. 7 μM each) were added to 100 μL of sample extract. Targeted bile acid measurement was performed using a QTRAP 5500 triple quadrupole mass spectrometer (Sciex, Darmstadt, Germany) coupled to an ExionLC AD (Sciex, Darmstadt, Germany) ultrahigh performance liquid chromatography system. A multiple reaction monitoring (MRM) method was used for the detection and quantification of the bile acids. An electrospray ion voltage of -4500 V and the following ion source parameters were used: curtain gas (35 psi), temperature ($450\text{ }^\circ\text{C}$), gas 1 (55 psi), gas 2 (65 psi), and entrance potential (-10 V). The MS parameters and LC conditions were optimized using commercially available standards of endogenous bile acids and deuterated bile acids, for the simultaneous quantification of selected 28 analytes. For separation of the analytes a $100 \times 2.1\text{ mm}$, 100 \AA , $1.7\text{ }\mu\text{m}$, Kinetex C18 column (Phenomenex, Aschaffenburg, Germany) was used. Chromatographic separation was performed with a constant flow rate of 0.4 mL/min using a mobile phase consisted of water (eluent A) and acetonitrile/water (95/5, v/v, eluent B), both containing 5 mM ammonium acetate and 0.1% formic acid. The gradient elution started with 25% B for 2 min, increased at 3.5 min to 27% B, in 2 min to 35% B, which was held until 10 min, increased in 1 min to 43% B, held for 1 min, increased in 2 min to 58% B; held 3 min isocratically at 58% B, then the concentration was increased to 65% at 17.5 min, with another increase to 80% B at 18 min, following an increase at 19 min to 100% B, which was held for 1 min, at 20.5 min the column was equilibrated for 4.5 min at starting. The injection volume for all samples was $1\text{ }\mu\text{L}$, the column oven temperature was set to $40\text{ }^\circ\text{C}$, and the auto-sampler was kept at $15\text{ }^\circ\text{C}$. Data acquisition and instrumental control were performed with Analyst 1.7 software (Sciex, Darmstadt, Germany) as previously described⁹⁰. Briefly, a standard curve (0.5 nM to 15000 nM, 16 points), linear regression and weighting type of $1/x$ was used to calculate BA concentrations⁹⁰. BAs measured are Cholic acid (CA), chenodeoxycholic acid (CDCA), a-Muricholic acid (aMCA), b-Muricholic acid (bMCA), Taurocholic acid (TCA), Taurochenodeoxycholic acid (TCDCa), Tauroursodeoxycholic acid (TUDCA), Taurohyodeoxycholic acid (THDCA), Tauroolithocholic acid (TLCA), Taurodeoxycholic acid (TDCA), Tauro-a-Muricholic acid (TaMCA), Glycochenodeoxycholic acid (GCDCA), Glycocholic acid (GCA), Deoxycholic acid (DCA), Lithocholic acid (LCA), y-Muricholic acid (y-MCA), 12-Dehydrocholic acid (12-DHCA), 12-Ketolithocholic acid (12-keto-LCA), 3-Dehydrocholic acid (3-DHCA), 6-Ketolithocholic acid (6-keto-LCA), 7-Dehydrocholic acid (7-DHCA), 7-Sulfocholic acid (7-sulfo-CA), Allocholic acid (ACA), Cholic acid-7 α -3one (CA-7 α -3one), Ursocholic acid (UCA), Dehydroolithocholic acid (DHLCA), Hyodeoxycholic acid (HDCA), Murideoxycholic acid (MDCA), Ursodeoxycholic acid (UDCA).

Targeted short-chain fatty acid measurement. For the quantitation of short-chain fatty acids (SCFAs) the 3-NPH method was used⁹¹. Briefly, 40 μL of the fecal extract and 15 μL of isotopically labeled standards (ca 50 μM) were mixed with 20 μL 120 mM EDC HCl-6% pyridine-solution and 20 μL of 200 mM 3-NPH HCl solution. After 30 min at $40\text{ }^\circ\text{C}$ and shaking at 1000 rpm using an Eppendorf Thermomix (Eppendorf, Hamburg, Germany), 900 μL acetonitrile/water (50/50, v/v) was added. After centrifugation at 13000 U/min for 2 min the clear supernatant was used for analysis. The same system as described above was used. The electrospray voltage was set to -4500 V , curtain gas to 35 psi, ion source gas 1 to 55, ion source gas 2 to 65 and the temperature to $500\text{ }^\circ\text{C}$. The MRM-parameters were optimized using commercially available standards for the SCFAs. The chromatographic separation was performed on a $100 \times 2.1\text{ mm}$, 100 \AA , $1.7\text{ }\mu\text{m}$, Kinetex C18 column (Phenomenex, Aschaffenburg, Germany) column with 0.1% formic acid (eluent A) and 0.1% formic acid in acetonitrile (eluent B) as elution solvents. An injection volume of $1\text{ }\mu\text{L}$ and a flow rate of 0.4 mL/min was used. The gradient elution started at 23% B which was held for 3 min, afterward the concentration was increased to

30% B at 4 min, with another increase to 40%B at 6.5 min, at 7 min 100% B was used which was hold for 1 min, at 8.5 min the column was equilibrated at starting conditions. The column oven was set to $40\text{ }^\circ\text{C}$ and the autosampler to $15\text{ }^\circ\text{C}$. Data acquisition and instrumental control were performed with Analyst 1.7 software (Sciex, Darmstadt, Germany). Concentrations of SCFA were calculated with the use of linear regression using a standard curve (ranging 0.0004 mM to 2 mM (12 points), SCFAs measured are Acetate, Propionate, Butyrate, Valeric acid, Desaminotyrosine and the Branched-chain Fatty acids (Isobutyric acid, 2-Methylbutyric acid and Isovaleric acid).

Targeted metabolite analyses. MultiQuant 3.0.3 Software (AB Sciex) was used to integrate the data and calculate the concentration. Isotopically labelled standards were used for SCFA quantitation. For bile acid quantitation, we used Dehydrocholic acid as internal standard to correct for losses during sample preparation and isotopically labelled references to correct for ionization effects during measurement, according to the paper of Sinah et al. 2021⁹⁰. For comparison between two groups, Mann-Whitney U test (two-sided) was used to test for statistical significance. Metabolite-microbiota correlation analyses were performed on relative abundance zOTU level within the rhythmic in male *Bmal1^{fl/fl}*, but not *Bmal1^{IEC-/-}* samples with at least a 30% prevalence. Spearman correlation and adjusted p-values between targeted metabolomics and zOTUs were calculated using the *rcor()* function in R. Correlation matrixes were visualized within the R package “corplot” v0.92 (Wei et al., 2017). Only correlations were plotted with a *p* value of <0.05 and coefficient values $R \leq -0.5$ and ≥ 0.5 . Furthermore, M2IA online platform⁹² was used for the global similarity analyses (PA plot) between metabolome and microbiota data.

Transfer experiments

Mice were gavaged with cecal microbiota at ZT13 from either cecal content (CT/ZT13) of *Bmal1^{IEC-/-}* mice ($n = 4$, mixture), or control mice kept in LD ($n = 5$, mixture), DD ($n = 4$) or starvation ($n = 5$) into germ-free wild type C57BL6 recipient mice at the age of 10 weeks. $100\text{ }\mu\text{L}$ of 7×10^6 bacteria/ μL were used for gavaging each mouse. Mice were weekly monitored for bodyweight changes and feces was sampled at week 5 after gavage in DNA stabilizer for 16 s analyses. Native fecal samples for targeted metabolomics were taken at ZT4 and ZT16. Afterwards, mice were sacrificed at the 2nd day in DD at CT13 at the age of 16 weeks. All mice were kept in the gnotobiology facility in isolators equipped with HEPA-filters at $22 \pm 1\text{ }^\circ\text{C}$ with a 12-h light/dark cycle (lights on 5 am till 5 pm). Mice were single housed and had ad libitum access to autoclaved chow (V1124-300, Sniff Diets, Soest, Germany) and autoclaved water.

Immune cell isolation from the lamina propria

Immune cells were isolated from freshly isolated jejunum and colon. Intestinal tissues were flipped, washed out and cut into 1 cm pieces. To remove epithelial cells, pieces were incubated in DMEM with 20 μL of 1 M DTT. After shaking for 15 minutes, tissues were incubated PBS with 200 μL of 150 mM EDTA at $37\text{ }^\circ\text{C}$ with shaking. After 3 times harsh shaking in Hanks buffer, jejunum tissue was then digested at $37\text{ }^\circ\text{C}$ for approximately 15 min in Thermoshake (200 rpm) with 0.6 mg/ml type VIII collagenase (Sigma-Aldrich). Colonic tissue was simultaneously digested under the same condition for approximately 25 min but with the mixture of 0.85 mg/ml type V collagenase (Sigma-Aldrich), 1.25 mg/ml collagenase D (Sigma-Aldrich), 10 $\mu\text{L}/\text{mL}$ Amphotericin (100x) 1 mg/ml Dispase II, and 30U/ml Deoxyribonuclease I (Sigma). Following digestion, intestinal cells were passed through a 40 μm strainer. Consequently, cells were fixed with 2% PFA, washed, and stored in RPMI at $4\text{ }^\circ\text{C}$ until further processing.

Fluorescence-activated cell sorting (FACS)

For intracellular stainings, cells were permeabilized with saponin 0.5% and stained with anti CD8 PE-, anti CD3 PerCP/Cy5.5, anti CD4 FITC-,

anti-IL-17a PE/cy7-, anti Infy- APC conjugated antibodies at dilution 1/100-1/50 for 30 min.

Surface stainings were performed using anti CD11c PE-, anti CD11b APC Cy7-, anti F4/80 PE/cy7-, anti Ly6G APC conjugated antibodies at dilution 1/50 for 30 minutes. Cells were analyzed on a LSR-II (BD Biosciences) flow cytometer and analysis was performed using FlowJo software (FlowJo, LLC, version 10.7.2). Gating strategies are illustrated in Supplementary Fig 7.

Histology

In formalin fixed tissues in paraffine were cut into 5µm thick slices and consequently stained according to the following steps: xylene/ 5 min, xylene/ 5 min, Ethanol 100%/ 5 min, Ethanol 100%/ 5 min, Ethanol 96%/ 2 min, Ethanol 96%/ 2 min, Ethanol 70%/ 2 min, Ethanol 70%/ 2 min, Water/ 30 s, hematoxylin/ 2 min, tap water/ 15 s, Scotts Tap Water/ 30 s, Water/ 30 s, Ethanol 96%/ 30 s, Eosin/ 30 s, Ethanol 96%/ 30 s, Ethanol 96%/ 30 s, Ethanol 100%/ 30 s, Ethanol 100%/ 30 s, Xylene/ 90 s, Xylene/ 90 s (Leica ST5020 multistainer). DPX new mounting media (Merck) was added to preserve the tissues. Stained slides were scanned and further analyzed for histological scoring. Histological scores were assessed blindly based on the degree of immune cell infiltration of all colonic wall layers (mucosa, submucosa and muscularis), crypt hyperplasia, goblet cell depletion and mucosal damage, resulting in a score from 0 (not inflamed) to 12 (severely inflamed) according to Katakura method⁹³.

Immunofluorescence staining of CD3

Antigens retrieval of the de-paraffinized and re-hydrated sections was performed by heating the slices in citrate buffer for 34 minutes. After multiple washing steps and tissues were blocked by donkey blocking buffer (1 h at room temperature and 1 hour at 4 °C). Tissue sections were incubated overnight with Anti E-cadherin (1:300, mouse, Abcam) anti-CD3 (1:400, rabbit, Sigma). Tissue were washed with PBS and followed by incubation with secondary antibodies (donkey antirabbit 546, donkey antimouse 647, both from Invitrogen with a dilution 1:200) for 1 h at room temperature. Finally, DAPI (Sigma) were used to stain the nuclei and then tissues were mounted using Aquatex. Sections were visualized with Fluoview FV10i microscope (Olympus, Shinjuku, Japan).

PICRUST 2.0

For prediction of functional of metagenomic functionality. Sequence of the gut controlled zOTUs, captured as described above, were used to construct the metagenome using PICRUST2.0⁹⁴. Corrected zOTU 16 s rRNA gene copy number is multiplied by the predicted functionality to predicted the metagenome. Resulted enzymatic genes classified according to Enzyme Commission (EC) numbers were mapped to Metacyc pathways. Superclasses were removed and Metacyc pathways abundance was used for statistical analysis using STAMP (2.1.3). Statistical differences were calculated based on White's non-parametric t-test and Benjamini Hochberg dales discovery rate to adjusted for multiple testing.

Statistical analyses

Statistical analyses were preformed using GraphPad Prism, version 9.0.0 (GraphPad Software), JTK_cycle v3.1.R²⁵ or R. With the use of the pipeline Rhea (Lagkourdos) between-sample microbiota diversity is calculated by generalized UniFrac using GUniFrac v1.1. distances. Quantification of GUniFrac distances was always done in comparison to ZT1 or CT1. Different in microbiota composition was calculated by PERMANOVA test on generalized Unifrac dissimilarity matrix and illustrated by MDS, The bar next to the graph indicate the dissimilarity for the distance of the bar⁸⁷. Circadian and diurnal patterns of individual 24 h period graphs, as well as phase calculation were analysed by fitting a cosine-wave equation: $y = \text{baseline} + (\text{amplitude} \cdot \cos(2 \cdot \pi \cdot ((x - [\text{phase shift}]/24))))$, with a fixed 24-h period for phyla, richness and single zOTU or by using the non-parametric algorithm JTK_cycle for

overall rhythmicity of all zOTUs. Connected straight lines in of individual 24 h period graphs within the figures indicate significant rhythmicity based on cosine analyses whereas dashed lines indicate non-significant cosine fit. Comparison of rhythm between data sets were preformed using an adjusted version of the Compare rhythm script²⁶, which performs JTK_cycle followed by DODR⁹⁵ available at (DOI: 10.5281/zenodo.7049842). Some CCGs when indicated were analysed with a harmonic - regression: $y = \text{baseline} + (\text{amplitude} A \cdot \cos(2 \cdot \pi \cdot ((x - [\text{phaseshift} A] / 24)))) + (\text{amplitude} B \cdot \cos(4 \cdot \pi \cdot ((x - [\text{phase shift} B] / 24))))$. Amplitude calculations depicted in the manhattan plots are based on the output of JTK_cycle and the phase was calculated by cosine-wave regression. Analysis between two groups was performed using the non-parametric Mann-Whitney test (two-sided). A *p* value ≤0.05 was assumed as statistically significant.

Heatmaps were generated using the online tool "heatmapper.ca"⁹⁶. Heatmaps were sorted based on peak phase of controls. Abundance plots were generated using SIAMCAT package (v1.10.0) in R using the "check.associations() function"⁹⁷. Visualisation of zOTUs and samples trees were conducted using the online platform "evolgenius.info"⁹⁸.

Reporting summary

Further information on research design is available in the Nature Research Reporting Summary linked to this article.

Data availability

The Microbiota sequencing data and metabolite data generated for this study have been deposited in Sequence Read Archive (SRA, submission ID: SUB10646422/Bioproject ID: PRJNA779969) and Zenodo (10.5281/zenodo.6962318). The processed data generated in this study are provided in the Supplementary Information and as a Source Data file. Cosine wave regression P values are provided in Supplementary data 5. Source data are provided with this paper.

Code availability

The modified version of the compare rhythm script is available (<https://doi.org/10.5281/zenodo.7049842>).

References

- Dunlap, J. C. Molecular bases for circadian clocks. *Cell* **96**, 271–290 (1999).
- Schibler, U., Ripperger, J. & Brown, S. A. Peripheral circadian oscillators in mammals: time and food. *J. Biol. Rhythms* **18**, 250–260 (2003).
- Duguay, D. & Cermakian, N. The crosstalk between physiology and circadian clock proteins. *Chronobiol. Int* **26**, 1479–1513 (2009).
- Zhang, R., Lahens, N. F., Ballance, H. I., Hughes, M. E. & Hogenesch, J. B. A circadian gene expression atlas in mammals: implications for biology and medicine. *Proc. Natl Acad. Sci. USA* **111**, 16219–16224 (2014).
- Pacha, J. & Sumova, A. Circadian regulation of epithelial functions in the intestine. *Acta Physiol. (Oxf.)* **208**, 11–24 (2013).
- Hoogerwerf, W. A. Role of clock genes in gastrointestinal motility. *Am. J. Physiol. Gastrointest. Liver Physiol.* **299**, G549–G555 (2010).
- Peterson, L. W. & Artis, D. Intestinal epithelial cells: regulators of barrier function and immune homeostasis. *Nat. Rev. Immunol.* **14**, 141–153 (2014).
- Segers, A. & Depoortere, I. Circadian clocks in the digestive system. *Nat. Rev. Gastroenterol. Hepatol.* **18**, 239–251 (2021).
- Leone, V. et al. Effects of diurnal variation of gut microbes and high-fat feeding on host circadian clock function and metabolism. *Cell host microbe* **17**, 681–689 (2015).
- Thaiss, C. A. et al. Transkingdom control of microbiota diurnal oscillations promotes metabolic homeostasis. *Cell* **159**, 514–529 (2014).

11. Zarrinpar, A., Chaix, A., Yooseph, S. & Panda, S. Diet and feeding pattern affect the diurnal dynamics of the gut microbiome. *Cell Metab.* **20**, 1006–1017 (2014).
12. Reitmeier, S. et al. Arrhythmic Gut Microbiome Signatures Predict Risk of Type 2 Diabetes. *Cell host microbe* **28**, 258–272 e256 (2020).
13. Liang, X., Bushman, F. D. & FitzGerald, G. A. Rhythmicity of the intestinal microbiota is regulated by gender and the host circadian clock. *Proc. Natl Acad. Sci. USA* **112**, 10479–10484 (2015).
14. Voigt, R. M. et al. The Circadian Clock Mutation Promotes Intestinal Dysbiosis. *Alcohol Clin. Exp. Res* **40**, 335–347 (2016).
15. Coleman, O. I. et al. Activated ATF6 Induces Intestinal Dysbiosis and Innate Immune Response to Promote Colorectal Tumorigenesis. *Gastroenterology* **155**, 1539–1552 e1512 (2018).
16. Lloyd-Price, J. et al. Multi-omics of the gut microbial ecosystem in inflammatory bowel diseases. *Nature* **569**, 655–662 (2019).
17. Turnbaugh, P. J. et al. An obesity-associated gut microbiome with increased capacity for energy harvest. *Nature* **444**, 1027–1031 (2006).
18. Ferraz-Bannitz, R. et al. Circadian Misalignment Induced by Chronic Night Shift Work Promotes Endoplasmic Reticulum Stress Activation Impacting Directly on Human Metabolism. *Biology (Basel)* **10** <https://doi.org/10.3390/biology10030197> (2021).
19. Gutierrez Lopez, D. E., Lashinger, L. M., Weinstock, G. M. & Bray, M. S. Circadian rhythms and the gut microbiome synchronize the host's metabolic response to diet. *Cell Metabol.* <https://doi.org/10.1016/j.cmet.2021.03.015> (2021).
20. Onalapo, A. Y. & Onalapo, O. J. Circadian dysrhythmia-linked diabetes mellitus: Examining melatonin's roles in prophylaxis and management. *World J. Diabetes* **9**, 99–114 (2018).
21. Voigt, R. M. et al. Circadian disorganization alters intestinal microbiota. *PLoS One* **9**, e97500 (2014).
22. Aschoff, J. Exogenous and endogenous components in circadian rhythms. *Cold Spring Harb. Symp. Quant. Biol.* **25**, 11–28 (1960).
23. Tourlousse, D. M. et al. Synthetic spike-in standards for high-throughput 16S rRNA gene amplicon sequencing. *Nucleic Acids Res* **45**, e23 (2017).
24. Thaiss, C. A. et al. Microbiota Diurnal Rhythmicity Programs Host Transcriptome Oscillations. *Cell* **167**, 1495–1510 e1412 (2016).
25. Hughes, M. E., Hogenesch, J. B. & Kornacker, K. JTK_CYCLE: an efficient nonparametric algorithm for detecting rhythmic components in genome-scale data sets. *J. Biol. Rhythms* **25**, 372–380 (2010).
26. Pelikan, A., Herzel, H., Kramer, A. & Ananthasubramanian, B. Venn diagram analysis overestimates the extent of circadian rhythm reprogramming. *FEBS J.* <https://doi.org/10.1111/febs.16095> (2021).
27. Thaben, P. F. & Westermark, P. O. Differential rhythmicity: detecting altered rhythmicity in biological data. *Bioinformatics* **32**, 2800–2808 (2016).
28. Damiola, F. et al. Restricted feeding uncouples circadian oscillators in peripheral tissues from the central pacemaker in the suprachiasmatic nucleus. *Genes Dev.* **14**, 2950–2961 (2000).
29. Coleman, O. I. & Haller, D. Bacterial Signaling at the Intestinal Epithelial Interface in Inflammation and Cancer. *Front Immunol.* **8**, 1927 (2017).
30. Wu, M. et al. The Dynamic Changes of Gut Microbiota in Muc2 Deficient Mice. *Int J Mol Sci* **19**, 92809 (2018).
31. Forman, R. A. et al. The goblet cell is the cellular source of the anti-microbial angiogenin 4 in the large intestine post *Trichuris muris* infection. *PLoS One* **7**, e42248 (2012).
32. Mukherji, A., Kobiita, A., Ye, T. & Chambon, P. Homeostasis in intestinal epithelium is orchestrated by the circadian clock and microbiota cues transduced by TLRs. *Cell* **153**, 812–827 (2013).
33. Kuang, Z. et al. The intestinal microbiota programs diurnal rhythms in host metabolism through histone deacetylase 3. *Science* **365**, 1428–1434 (2019).
34. Wang, Y. et al. The intestinal microbiota regulates body composition through NFIL3 and the circadian clock. *Science* **357**, 912–916 (2017).
35. Hardbower, D. M. et al. Arginase 2 deletion leads to enhanced M1 macrophage activation and upregulated polyamine metabolism in response to *Helicobacter pylori* infection. *Amino Acids* **48**, 2375–2388 (2016).
36. Biddle, A., Stewart, L., Blanchard, J. & Leschine, S. Untangling the Genetic Basis of Fibrolytic Specialization by Lachnospiraceae and Ruminococcaceae in Diverse Gut Communities. *Diversity* **5**, 627–640 (2013).
37. Ridlon, J. M., Kang, D. J., Hylemon, P. B. & Bajaj, J. S. Bile acids and the gut microbiome. *Curr. Opin. Gastroenterol.* **30**, 332–338 (2014).
38. Ericsson, A. C., Personett, A. R., Turner, G., Dorfmeier, R. A. & Franklin, C. L. Variable Colonization after Reciprocal Fecal Microbiota Transfer between Mice with Low and High Richness Microbiota. *Front Microbiol* **8**, 196 (2017).
39. Gundersen, M. D. et al. Loss of interleukin 33 expression in colonic crypts - a potential marker for disease remission in ulcerative colitis. *Sci. Rep.* **6**, 35403 (2016).
40. Liu, T., Zhang, L., Joo, D. & Sun, S. C. NF-kappaB signaling in inflammation. *Signal. Transduct. Target. Ther.* **2** <https://doi.org/10.1038/sigtrans.2017.23> (2017).
41. Hooper, L. V., Stappenbeck, T. S., Hong, C. V. & Gordon, J. I. Angiogenins: a new class of microbicidal proteins involved in innate immunity. *Nat. Immunol.* **4**, 269–273 (2003).
42. Mardinoglu, A. et al. The gut microbiota modulates host amino acid and glutathione metabolism in mice. *Mol. Syst. Biol.* **11**, 834 (2015).
43. Wu, G. et al. Light exposure influences the diurnal oscillation of gut microbiota in mice. *Biochem Biophys Res Commun.* **501**, 16–23 (2018).
44. Deaver, J. A., Eum, S. Y. & Toborek, M. Circadian Disruption Changes Gut Microbiome Taxa and Functional Gene Composition. *Front Microbiol* **9**, 737 (2018).
45. Frazier, K. et al. High fat diet disrupts diurnal interactions between REG3g and small intestinal gut microbes resulting in metabolic dysfunction. *bioRxiv* (2020).
46. Alenghat, T. et al. Histone deacetylase 3 coordinates commensal-bacteria-dependent intestinal homeostasis. *Nature* **504**, 153–157 (2013).
47. Caricilli, A. M. et al. Gut microbiota is a key modulator of insulin resistance in TLR 2 knockout mice. *PLoS Biol.* **9**, e1001212 (2011).
48. Wu, S. E. et al. Microbiota-derived metabolite promotes HDAC3 activity in the gut. *Nature* **586**, 108–112 (2020).
49. Schroeder, B. O. Fight them or feed them: how the intestinal mucus layer manages the gut microbiota. *Gastroenterol. Rep. (Oxf.)* **7**, 3–12 (2019).
50. Bishehsari, F., Voigt, R. M. & Keshavarzian, A. Circadian rhythms and the gut microbiota: from the metabolic syndrome to cancer. *Nat. Rev. Endocrinol.* **16**, 731–739 (2020).
51. Tailford, L. E., Crost, E. H., Kavanaugh, D. & Juge, N. Mucin glycan foraging in the human gut microbiome. *Front Genet* **6**, 81 (2015).
52. Carr, F. J., Chill, D. & Maida, N. The lactic acid bacteria: a literature survey. *Crit. Rev. Microbiol* **28**, 281–370 (2002).
53. Gerard, P. Metabolism of cholesterol and bile acids by the gut microbiota. *Pathogens* **3**, 14–24 (2013).
54. Beli, E., Prabakaran, S., Krishnan, P., Evans-Molina, C. & Grant, M. B. Loss of Diurnal Oscillatory Rhythms in Gut Microbiota Correlates with Changes in Circulating Metabolites in Type 2 Diabetic db/db Mice. *Nutrients* **11**, 102310 (2019).
55. Govindarajan, K. et al. Unconjugated Bile Acids Influence Expression of Circadian Genes: A Potential Mechanism for Microbe-Host Crosstalk. *PLoS One* **11**, e0167319 (2016).
56. Vavassori, P., Mencarelli, A., Renga, B., Distrutti, E. & Fiorucci, S. The bile acid receptor FXR is a modulator of intestinal innate immunity. *J. Immunol.* **183**, 6251–6261 (2009).

57. Kim, M. H., Kang, S. G., Park, J. H., Yanagisawa, M. & Kim, C. H. Short-chain fatty acids activate GPR41 and GPR43 on intestinal epithelial cells to promote inflammatory responses in mice. *Gastroenterology* **145**, 396–406 (2013). e391-310.
58. Segers, A. et al. The circadian clock regulates the diurnal levels of microbial short-chain fatty acids and their rhythmic effects on colon contractility in mice. *Acta Physiol. (Oxf.)* **225**, e13193 (2019).
59. Bhutta, H. Y. et al. Effect of Roux-en-Y gastric bypass surgery on bile acid metabolism in normal and obese diabetic rats. *PLoS One* **10**, e0122273 (2015).
60. Haeusler, R. A., Astiarraga, B., Camastra, S., Accili, D. & Ferrannini, E. Human insulin resistance is associated with increased plasma levels of 12 α -hydroxylated bile acids. *Diabetes* **62**, 4184–4191 (2013).
61. Brufau, G. et al. Improved glycemic control with colessevelam treatment in patients with type 2 diabetes is not directly associated with changes in bile acid metabolism. *Hepatology* **52**, 1455–1464 (2010).
62. Zheng, X. et al. Hyocholic acid species as novel biomarkers for metabolic disorders. *Nat. Commun.* **12**, 1487 (2021).
63. Yoshimoto, S. et al. Obesity-induced gut microbial metabolite promotes liver cancer through senescence secretome. *Nature* **499**, 97–101 (2013).
64. Ozcan, U. et al. Chemical chaperones reduce ER stress and restore glucose homeostasis in a mouse model of type 2 diabetes. *Science* **313**, 1137–1140 (2006).
65. Kars, M. et al. Tauroursodeoxycholic Acid may improve liver and muscle but not adipose tissue insulin sensitivity in obese men and women. *Diabetes* **59**, 1899–1905 (2010).
66. Jia, W., Xie, G. & Jia, W. Bile acid-microbiota crosstalk in gastrointestinal inflammation and carcinogenesis. *Nat. Rev. Gastroenterol. Hepatol.* **15**, 111–128 (2018).
67. Narimatsu, K. et al. Toll-like receptor (TLR) 2 agonists ameliorate indomethacin-induced murine ileitis by suppressing the TLR4 signaling. *J. Gastroenterol. Hepatol.* **30**, 1610–1617 (2015).
68. Maslowski, K. M. et al. Regulation of inflammatory responses by gut microbiota and chemoattractant receptor GPR43. *Nature* **461**, 1282–1286 (2009).
69. Barker, N. et al. Identification of stem cells in small intestine and colon by marker gene Lgr5. *Nature* **449**, 1003–1007 (2007).
70. Bamias, G. et al. Intestinal-specific TNF α overexpression induces Crohn's-like ileitis in mice. *PLoS One* **8**, e72594 (2013).
71. Rakoff-Nahoum, S., Paglino, J., Eslami-Varzaneh, F., Edberg, S. & Medzhitov, R. Recognition of commensal microflora by toll-like receptors is required for intestinal homeostasis. *Cell* **118**, 229–241 (2004).
72. Valentini, M. et al. Immunomodulation by gut microbiota: role of Toll-like receptor expressed by T cells. *J. Immunol. Res* **2014**, 586939 (2014).
73. Xiao, Y. et al. Interleukin-33 Promotes REG3 γ Expression in Intestinal Epithelial Cells and Regulates Gut Microbiota. *Cell Mol. Gastroenterol. Hepatol.* **8**, 21–36 (2019).
74. Dou, X. et al. TLR2/4-mediated NF- κ B pathway combined with the histone modification regulates beta-defensins and interleukins expression by sodium phenyl butyrate in porcine intestinal epithelial cells. *Food Nutr Res* **62**, 1493 (2018).
75. Zheng, D., Liwinski, T. & Elinav, E. Interaction between microbiota and immunity in health and disease. *Cell Res* **30**, 492–506 (2020).
76. Metwaly, A. et al. Integrated microbiota and metabolite profiles link Crohn's disease to sulfur metabolism. *Nat. Commun.* **11**, 4322 (2020).
77. Kawai, M. et al. Intestinal clock system regulates skeletal homeostasis. *JCI Insight* **4** <https://doi.org/10.1172/jci.insight.121798> (2019).
78. Ubeda, C. et al. Familial transmission rather than defective innate immunity shapes the distinct intestinal microbiota of TLR-deficient mice. *J. Exp. Med* **209**, 1445–1456 (2012).
79. Jud, C., Schmutz, I., Hampp, G., Oster, H. & Albrecht, U. A guideline for analyzing circadian wheel-running behavior in rodents under different lighting conditions. *Biol. Proced. Online* **7**, 101–116 (2005).
80. Li, Z. et al. Essential roles of enteric neuronal serotonin in gastrointestinal motility and the development/survival of enteric dopaminergic neurons. *J. Neurosci.* **31**, 8998–9009 (2011).
81. Godon, J. J., Zumstein, E., Dabert, P., Habouzit, F. & Moletta, R. Molecular microbial diversity of an anaerobic digester as determined by small-subunit rDNA sequence analysis. *Appl Environ. Microbiol.* **63**, 2802–2813 (1997).
82. Edgar, R. C. Search and clustering orders of magnitude faster than BLAST. *Bioinformatics* **26**, 2460–2461 (2010).
83. Edgar, R. C., Haas, B. J., Clemente, J. C., Quince, C. & Knight, R. UCHIME improves sensitivity and speed of chimera detection. *Bioinformatics* **27**, 2194–2200 (2011).
84. Edgar, R. C. UNOISE2: improved error-correction for Illumina 16S and ITS amplicon sequencing. *bioRxiv*, 081257: <https://doi.org/10.1101/081257>. (2016).
85. Edgar, R. C. Updating the 97% identity threshold for 16S ribosomal RNA OTUs. *Bioinformatics* **34**, 2371–2375 (2018).
86. Yoon, S. H. et al. Introducing EzBioCloud: a taxonomically united database of 16S rRNA gene sequences and whole-genome assemblies. *Int. J. Syst. Evol. Microbiol.* **67**, 1613–1617 (2017).
87. Lagkouvardos, I., Fischer, S., Kumar, N. & Clavel, T. Rhea: a transparent and modular R pipeline for microbial profiling based on 16S rRNA gene amplicons. *PeerJ* **5**, e2836 (2017).
88. Kumar, S., Stecher, G., Li, M., Niyaz, C. & Tamura, K. MEGA X: Molecular Evolutionary Genetics Analysis across Computing Platforms. *Mol. Biol. Evol.* **35**, 1547–1549 (2018).
89. Subramanian, B., Gao, S., Lercher, M. J., Hu, S. & Chen, W.-H. Evolvew v3: a webserver for visualization, annotation, and management of phylogenetic trees. *Nucleic Acids Res.* **47**, W270–W275 (2019).
90. Reiter, S. et al. Development of a Highly Sensitive Ultra-High-Performance Liquid Chromatography Coupled to Electrospray Ionization Tandem Mass Spectrometry Quantitation Method for Fecal Bile Acids and Application on Crohn's Disease Studies. *J. Agric. Food Chem.* **69**, 5238–5251 (2021).
91. Han, J., Lin, K., Sequeira, C. & Borchers, C. H. An isotope-labeled chemical derivatization method for the quantitation of short-chain fatty acids in human feces by liquid chromatography-tandem mass spectrometry. *Anal. Chim. Acta* **854**, 86–94 (2015).
92. Ni, Y. et al. M2IA: a web server for microbiome and metabolome integrative analysis. *Bioinformatics* **36**, 3493–3498 (2020).
93. Katakura, K. et al. Toll-like receptor 9-induced type I IFN protects mice from experimental colitis. *J. Clin. Invest* **115**, 695–702 (2005).
94. Douglas, G. M. et al. PICRUSt2 for prediction of metagenome functions. *Nat. Biotechnol.* **38**, 685–688 (2020).
95. Singer, J. M. & Hughey, J. J. LimoRhyde: A Flexible Approach for Differential Analysis of Rhythmic Transcriptome Data. *J. Biol. Rhythms* **34**, 5–18 (2019).
96. Babicki, S. et al. Heatmapper: web-enabled heat mapping for all. *Nucleic Acids Res* **44**, W147–W153 (2016).
97. Wirbel, J. et al. Microbiome meta-analysis and cross-disease comparison enabled by the SIAMCAT machine-learning toolbox. *bioRxiv*, 2020.2002.2006.931808 <https://doi.org/10.1101/2020.02.06.931808> (2020).

Acknowledgements

This work was supported by the Technical University of Munich, providing funding for the ZIEL Institute for Food & Health, animal facility support, technical assistance and support for 16S rRNA gene amplicon sequencing. Moreover, SK was supported by the German Research Foundation (DFG, project KI 19581) and the European Crohn's and Colitis Organisation (ECCO, grant 5280024). SK and DH received funding by

the Funded by the Deutsche Forschungsgemeinschaft (DFG, German Research Foundation) – Project number 395357507 – SFB 1371). We are thankful for J. Bruder and Z. Fras providing assistance with animal experiments and preliminary data collection.

Author contributions

S.K. conceived and coordinated the project. M.H., BA. performed mouse experiments and fecal samples collection. B.A., M.H. and Y.N. provided tissue samples and performed gene expression analysis. S.K. and M.H. analyzed activity and food intake behavior. M.H., B.A., S.R. and S.K. performed 16 S rRNA gene sequencing and bioinformatics analysis. B.A. and M.H. analyzed predicted microbial functionality. Y.N. performed FACS analyses. M.H. and K.K. performed targeted metabolomics and data analysis. SK supervised the work and data analysis. S.K. and D.H. secured funding. M.H., B.A., D.H. and S.K. wrote the manuscript. All authors reviewed and revised the manuscript. MH and BA contributed equally to this work.

Funding

Open Access funding enabled and organized by Projekt DEAL.

Competing interests

The authors declare no competing interests.

Additional information

Supplementary information The online version contains supplementary material available at <https://doi.org/10.1038/s41467-022-33609-x>.

Correspondence and requests for materials should be addressed to Silke Kiessling.

Peer review information *Nature Communications* thanks the anonymous reviewers for their contribution to the peer review of this work.

Reprints and permission information is available at <http://www.nature.com/reprints>

Publisher's note Springer Nature remains neutral with regard to jurisdictional claims in published maps and institutional affiliations.

Open Access This article is licensed under a Creative Commons Attribution 4.0 International License, which permits use, sharing, adaptation, distribution and reproduction in any medium or format, as long as you give appropriate credit to the original author(s) and the source, provide a link to the Creative Commons license, and indicate if changes were made. The images or other third party material in this article are included in the article's Creative Commons license, unless indicated otherwise in a credit line to the material. If material is not included in the article's Creative Commons license and your intended use is not permitted by statutory regulation or exceeds the permitted use, you will need to obtain permission directly from the copyright holder. To view a copy of this license, visit <http://creativecommons.org/licenses/by/4.0/>.

© The Author(s) 2022